Future vegetation-climate interactions in Eastern Siberia: an assessment of the competing effects of CO_2 and secondary organic aerosols

A Arneth[1,*], R Makkonen[2], S Olin[3], P Paasonen[2], T Holst[3], MK Kajos[2], M Kulmala[2], T Maximov[4], PA Miller[3], G. Schurgers[3,5]

[1] Karlsruhe Institute of Technology, Institute of Meteorology and Climate Research/Atmospheric Environmental Research, Garmisch Partenkirchen, Germany

[2] Department of Physics, University of Helsinki, P.O. Box 64, 00014 University of Helsinki, Finland

[3] Department of Physical Geography and Ecosystem Science, Lund University, Sölvegatan 12, 22362 Lund, Sweden

[4] Department of Plant Ecological Physiology and Biochemistry Lab., Institute for Biological Problems of Cryolithozone SB RAS, 41, Lenin ave, Yakutsk 677980, Russia

[5] Department of Geosciences and Natural Resource Management, University of Copenhagen, Øster Voldgade 10, 1350 Copenhagen, Denmark

*: almut.arneth@kit.edu

Abstract

Disproportional warming in the northern high latitudes, and large carbon stocks in boreal and (sub)arctic ecosystems have raised concerns as to whether substantial positive climate feedbacks from biogeochemical process responses should be expected. Such feedbacks occur if increasing temperatures lead to e.g., a net release of CO_2 or CH_4. However, temperature-enhanced emissions of biogenic volatile organic compounds (BVOC) have been shown to contribute to the growth of secondary organic aerosol (SOA) which is known to have a negative radiative climate effect. Combining measurements in Eastern Siberia with model-based estimates of vegetation and permafrost dynamics, BVOC emissions and aerosol growth, we assess here possible future changes in ecosystem CO_2 balance and BVOC-SOA interactions, and discuss these changes in terms of possible climate effects. Globally, the effects of changes in Siberian ecosystem CO_2 balance and SOA formation are small, but when concentrating on Siberia and the northern hemisphere the negative forcing from changed aerosol direct and indirect effects become notable – even though the associated temperature response would not necessarily follow a similar spatial pattern. While our analysis does not include other important processes that are of relevance for the climate system, the CO_2 and BVOC-SOA interplay serves as an example for the complexity of the interactions between emissions and vegetation dynamics that underlie individual terrestrial feedbacks and highlights the importance of addressing ecosystem-climate feedbacks in consistent, process-based model frameworks.

1. Introduction

Warming effects on ecosystem carbon cycling in northern ecosystems (Serreze et al., 2000;Tarnocai et al., 2009), and the potential for large climate-feedbacks from losses of CO_2 or CH_4 from these carbon-dense systems have been widely discussed (Khvorostyanov et al., 2008; Schuur et al., 2009; Arneth et al., 2010). Other biogeochemical processes can also lead to feedbacks, in particular through emissions of biogenic volatile organic compounds (BVOC) that are important precursors for tropospheric O_3 formation, affect methane lifetime and also act as precursors for secondary organic aerosol (SOA). These latter interactions with SOA have a cooling effect (Arneth et al., 2010; Makkonen et al., 2012b; Paasonen et al., 2013). Condensation of monoterpenes (*MT*), a group of BVOC with large source strength from coniferous vegetation, on pre-existing particles increases the observed particle mass, as well as the number of particles large enough to act as cloud condensation nuclei (CCN; equivalent to particles > *ca.* 100 nm) at boreal forest sites (Tunved et al., 2006). For present-day conditions, Spracklen et al. (2008a) estimated a radiative cooling of -1.8 to -6.7 W per m^{-2} of boreal forest area from the BVOC-SOA interplay.

How future changes in *MT* emissions affect SOA growth and climate is very uncertain. This is partially because of the lack of process-understanding of the various steps of aerosol formation and growth, and interactions with cloud formation (Hallquist et al., 2009; Carslaw et al., 2010), and partially because the issue of how spatial patterns of changing emissions of atmospherically rapidly reactive substances translate into a changing patterns

of radiative forcing, and then into a surface temperature change, has not yet been resolved (Shindell et al., 2008; Fiore et al., 2012).

The Russian boreal forest represents the largest continuous conifer region in the world. About one third of this forested area (ca. 730 X 10^6 ha) is dominated by larch (Shvidenko et al., 2007), in particular by the *Larix gmelinii* and *L. cajanderii* forests growing east of the Yenisei river on permafrost soils. Despite its vast expanse, the first seasonal measurements of *MT* emissions from Eastern Siberian larch have only recently been published (Kajos et al., 2013). Leaf *MT* emission capacities are highly species-dependent, thus any model estimate of *MT* emissions from boreal larch forests that rely solely on generic BVOC emission parameterisations obtained from other conifer species will give inaccurate emission and related SOA aerosol number concentrations for this region (Spracklen et al., 2008a). We therefore provide here a first assessment of *MT* emission rates from the Eastern Siberian larch biome, combining measured emission capacities with a process-based dynamic vegetation model and quantitatively linking *MT* emissions and SOA formation. We use the observations and process-models to assess climate change effects on future vegetation composition, BVOC emissions and the concentration of particles of CCN size. We discuss how the climate impact of future SOA levels from changes in BVOC emissions across Eastern Siberia compares with changes in the regional CO_2 balance. The chief goal of the study was not to provide a full surface climate-feedback quantification (for which today's global coupled modelling-tools are insufficient) but rather to highlight the number of potentially opposing processes that need to be covered when doing so.

2. Methods

2.1 Site description, BVOC and aerosol measurements

Leaf BVOC emissions fluxes, above canopy monoterpene concentration and aerosol particle size and number concentration were measured during the growing season 2009 at the research station Spasskaya Pad, located ca. 40km to the northeast of Yakutsk (62°15'18.4"N, 129°37'07.9"E) and centred in the Eastern Siberian larch biome (Kobak et al., 1996;Tchebakova et al., 2006). In the northern direction, no major pollution sources exist within hundreds of km, the nearest mining areas are concentrated to the south and west of Yakutsk. The predominant air flow to the site is either from southern (via Yakutsk) or northern locations. Forest fires contribute to aerosol load in summer.

An eddy covariance tower for measurements of forest-atmosphere exchange of CO_2, water vapour and sensible heat was established at Spasskaya Pad in the late 1990s (Ohta et al., 2001;Dolman et al., 2004) in a *L. cajanderii* forest growing on permafrost soil with an understory vegetation consisting of ericaceous shrubs. The forest has an average age of ca. 185 years and canopy height is little less than 20 m. Maximum one-sided larch leaf area index in summer is around two (Ohta et al., 2001, Takeshi et al., 2008). In 2009, leaf samples for BVOC analyses were taken, accessing the upper part of the canopy from a scaffolding tower located within few hundred metres of the eddy flux tower (Kajos et al., 2013). Using a custom-made Teflon branch chamber, air filtered of O_3 was sampled onto Tenax-TA/Carbopack-B cartridges with a flow rate of 220 ml min^{-1}. A total of 5-12 samples were taken during the day, from two trees on south-facing branches approximately 2 m below the tree top. The cartridge samples were stored at 5°C during the campaigns, transported afterwards to Helsinki

and thermally desorbed and analysed using a thermal desorption instrument (Perkin-Elmer TurboMatrix 650, Waltham, USA) attached to a gas-chromatograph (Perkin-Elmer Clarus 600, Waltham, USA). For details on chamber, adsorbents and laboratory measurements, see (Haapanala et al., 2009;Ruuskanen et al., 2007;Hakola et al., 2006).

Monoterpene concentrations and forest-atmosphere exchange fluxes were measured with a high-sensitive Quadrupole PTR-MS (Ionicon, Innsbruck, Austria) located in a hut at the foot of the eddy covariance tower. Sample air was drawn through a heated PFA tube using a 20 l min-1 flow from the inlet located at 30.3m above ground. While reporting here on monoterpenes only, a range of masses, corresponding to BVOCs (e.g., isoprene, methanol, acetaldehyde) were sampled sequentially, with typical dwell times of 0.5 s and scanning sequences of around 4s. Measurement set-up, disjunct eddy covariance flux calculations, and quality control followed Holst et al. (2010). It was not possible to import a gas calibration standard to Spasskaya Pad due to security and customs restrictions, and thus the PTR-MS could not be calibrated on-site. However, the instrument had been calibrated before and after the field campaign using a gas standard mixture from Ionimed (Innsbruck, Austria) using the same detector and instrument settings as during the field campaigns.

Aerosol particles were continuously monitored with a Scanning mobility particle sizer (SMPS) located at the foot of the eddy covariance tower, connected to a Differential mobility analyzer (DMA; Hauke type: medium; custom built; for size segregation of aerosol particles) in front of a Condensation Particle Counter (CPC; 3010, TSI Inc. USA; for determining the number of the size segregated particles). The system was identical to the one described and evaluated in (Svenningsson et al., 2008). Scans across the size range of 6 – 600 nm were completed every 5 minutes. The SMPS data were used to determine occasions of aerosol particle nucleation. The growth rates were calculated from log-normal modes fitted to the measured particle size distribution following Hussein et al. (2005). The time evolution of the diameters at which the fitted modes peaked was inspected visually, and the growth rate was determined with linear least squares fitting to these peak diameters whenever a continuous increase in diameter was observed. In this analysis we calculated growth rates for particles from 25 to 160 nm.

The source rate for condensing vapour (Q, molecules cm^3 s^{-1}) was determined by calculating the concentration of condensable vapour needed to produce the observed growth rate (C_{GR}, cm^{-3}, Nieminen et al., 2010) and the condensation sink from the particle size distribution (CS, s^{-1}, Kulmala et al., 2001). In steady state the sources and sinks for the condensing vapour are equal, and thus we determined the source rate as $Q=C_{GR}\bullet$CS.

2.2 Modelling of dynamic vegetation processes, permafrost and BVOC emissions

We applied the dynamic global vegetation model (DGVM) LPJ-GUESS (Smith et al., 2001; Sitch et al., 2003), including algorithms to compute canopy BVOC emission following (Niinemets et al., 1999;Arneth et al., 2007b;Schurgers et al., 2009a), and permafrost as adopted from Wania et al. (2009) (Table 1). LPJ-GUESS simulates global and regional dynamics and composition of vegetation in response to changes in climate and atmospheric CO_2 concentration. Physiological processes like photosynthesis, autotrophic and heterotrophic respiration are calculated explicitly, a set of carbon allocation rules determines plant growth. Plant establishment, growth, mortality, and decomposition, and their response to resource availability (light, water)

136 modulate seasonal and successional population dynamics arising from a carbon allocation trade-off (Smith et
137 al., 2001). Fire disturbance is included in the model (Thonicke et al., 2001). Similar to other DGVMs, a number
138 of plant functional types (PFT) are specified to represent the larger global vegetation units (Sitch et al., 2003).
139 BVOC emissions models, whether these are linked to DGVMs or to a prescribed vegetation map, all rely
140 on using emission potentials (*E**, leaf emissions at standardised environmental conditions) or some derivatives
141 in their algorithms. In LPJ-GUESS, production and emissions of leaf and canopy isoprene and monoterpenes
142 are linked to their photosynthetic production, specifically the electron transport rate, and the requirements for
143 energy and redox-equivalents to produce a unit of isoprene from triose-phosphates (Niinemets et al., 1999;
144 Arneth et al., 2007b; Schurgers et al., 2009a). A specified fraction of absorbed electrons used for isoprene
145 (monoterpene) production (ε) provides the link to PFT-specific *E** (Arneth et al., 2007a); in case of
146 monoterpenes emitted from storage an additional correction is applied to account for their light-dependent
147 production (taking place over parts of the day) and temperature-driven (taking place the entire day) emissions
148 (Schurgers et al., 2009a). Half of the produced monoterpenes were stored, whereas the other half was emitted
149 directly (Schurgers et al., 2009a). Values for *E** similar to the global parameterisation for most of the model's
150 PFTs (Schurgers et al., 2009a), with exception of boreal needle-leaf summergreen (BNS) "larch" PFT (see
151 results).
152 Contrasting the stimulation of BVOC emissions in a warmer and more productive environment, higher CO_2
153 concentrations have been shown to inhibit leaf isoprene production. Even though the underlying metabolic
154 mechanism is not yet fully understood, this effect has been observed in a number of studies (for an overview
155 see Figure 6 in Arneth et al., 2011). Due to limited experimental evidence, whether or not a similar response
156 occurs in monoterpene producing species cannot yet be confirmed, especially in species that emit from storage.
157 The model is set-up to test this hypothesis. Arneth et al. (2007a) proposed an empirical function for CO_2-
158 inhibition, based on the ratio of leaf internal CO_2 concentration at a standard atmospheric CO_2 level (taken as
159 370ppm) and at the given atmospheric CO_2 levels of the simulation year (both calculated for non-water-
160 stressed conditions); the relationships has been shown since to fit an updated compilation of observations well
161 (Arneth et al., 2011). The algorithm that describes the CO_2-inhibition of BVOC emission can either be enabled
162 or disabled in the model (Arneth et al., 2007a) and simulations results thus compared (see Figure A1,
163 Appendix; Table 2).
164 LPJ-GUESS was recently expanded with a permafrost module following Wania et al. (Wania et al.,
165 2009;Miller and Smith, 2012) in which a numerical solution of the heat diffusion equation was introduced.
166 The soil column in LPJ-GUESS now consists of a snow layer of variable thickness, a litter layer of fixed
167 thickness (5 cm), and a soil column of depth 2 m (with sublayers of thickness 0.1 m) from which plants can
168 extract non-frozen water above the wilting point. A "padding" column of depth 48 m (with thicker sublayers)
169 is also present beneath these three layers to aid in the accurate simulation of temperatures in the overlying
170 compartments (Wania et al., 2009). Soil temperatures throughout the soil column are calculated daily, and
171 change in response to changing surface air temperature and precipitation input, as well as the insulating effects
172 of the snow layer and phase changes in the soil's water.

Here we run the model with 0.5 degree spatial resolution, using climate and atmospheric CO_2 as driving variables as described in the literature (Smith et al., 2001). Values describing growth and survival of the BNS "larch" PFT were adopted from previous studies (Sitch et al., 2003; Hickler et al., 2012; Miller and Smith, 2012), but with the degree-day cumulative temperature requirements on a five-degree basis (GDD5) to attain full leaf cover reduced from 200 to 100 (Moser et al., 2012). Minimum GDD5 to allow establishment was set to 350 resulting in establishment of seedlings in very cold locations. Soil thermal conductivity was 2 $Wm^{-1} K^{-1}$. The model was spun up for 500 years to 1900 values using CO_2 concentration from the year 1900 and repeating de-trended climate from 1901-1930 from CRU (Mitchell and Jones, 2005). Historical (20^{th} century) simulations used observed CO_2 concentrations and based on variable CRU climate. Simulations for the 21^{st} century were based on ECHAM climate, using RCP 8.5 emissions (Riahi et al., 2007). The model requires daily radiation, precipitation and maximum and minimum air temperatures as input (Arneth et al., 2007b). The generated GCM climate was interpolated to the CRU half-degree grid, and monthly values interpolated to daily ones (see Ahlström et al., 2012, and references therein). These daily fields were then bias-corrected using the years 1961-1990 as reference period, as in Ahlström et al. (2012). CO_2 inhibition of BVOC emissions were switched on and off in separate simulations to assess the sensitivity of our results to this process. Totals across Siberia were calculated for a grid-box that ranged from 46 to 71 ^{o}N and 76 to 164 ^{o}E. Simulated changes in total carbon uptake or losses were translated into radiative forcing following (IPCC, 2007), assuming a 50% uptake in oceans in case of a net loss to the atmosphere (Sitch et al., 2007).

2.3 Modelling aerosols and CCN

To model the effect of BVOCs on CCN concentrations, we use the global aerosol-climate model ECHAM5.5-HAM2 (Zhang et al., 2012). ECHAM5.5-HAM2 includes the aerosol components of black carbon, organic carbon, dust, sea salt and sulfate (Table 1) , and describes the aerosol size distribution with seven log-normal modes. The microphysics module M7 (Vignati et al., 2004) includes nucleation, coagulation and condensation. In this study, we use the ECHAM5.5-HAM2 version with activation-type as described in Makkonen et al. (Makkonen et al., 2012). For simulating secondary organic aerosol, we use the recently developed SOA module (Jokinen et al., 2015). The SOA module explicitly accounts for gas-phase formation of extremely low volatility organic compounds (ELVOCs) from monoterpene oxidation. The module implements a hybrid mechanism for SOA formation: ELVOCs are assumed to condense to the aerosol population according to the Fuchs-corrected condensation sink, while semi-volatile organic compounds (SVOCs) are partitioned according to organic aerosol mass. While simulated ELVOCs are able to partition more effectively to nucleation and Aitken mode, hence providing growth for nucleated particles to CCN size, SVOCs primarily add organic mass to accumulation and coarse aerosol modes. A total SOA yield of 15% from monoterpenes is assumed (Dentener et al., 2006). While similar assumption on total SOA yield is applied by most aerosol-climate models, the simulated SOA is likely to be underestimated (e.g., Tsigaridis et al., 2014).

ECHAM5.5-HAM2 was run with different BVOC emission scenarios in year 2000 and 2100 simulated offline with LPJ-GUESS (see previous section). The model is using T63 spectral resolution with 31 vertical hybrid sigma levels. The simulations apply present-day oxidant fields as in Stier et al. (2005). All simulations are initiated with a six months spin-up, followed by 5 years of simulation for analysis. The model climate is

nudged towards ERA-40 reanalysis year 2000 meteorology, an approach that is widely used in aerosol-climate assessments (Zhang et al., 2014). Present-day wildfire and anthropogenic aerosol and precursor emissions are applied for all simulations (Dentener et al., 2006). One of the foci here are BVOC, comparing present-day and future BVOC emissions (choosing a conservative estimate of E^*=1.9 μg C m^{-2}(leaf) h^{-1}, see results section for further detail on E^* but keeping other emissions constant (oxidant fields and nudging meteorology are same for both 2000 and 2100). The emissions of dust and sea salt are modelled interactively (Zhang et al., 2012).

The analysis of model results includes total particle number concentration (CN) and cloud condensation nuclei at 1% supersaturation (CCN(1%)), since it reflects the changes in Aitken mode concentrations and local changes in precursor emissions. While "realistic" supersaturations are generally lower, choosing CCN(1.0%) concentration provides the upper limit for CCN concentrations. The simulations are also used to assess the radiative effects of SOA. In the simulations, the aerosol concentrations are interactively coupled to the cloud-microphysics scheme (Lohmann et al., 2007) and to the direct aerosol radiative calculation. The aerosol indirect effect is evaluated as a change in cloud radiative forcing (ΔCRF). The direct aerosol effect accounts only for clear-sky short-wave forcing (ΔCSDRF). The radiative effects are calculated as differences from two time-averaged 5-year simulations as

$\Delta CRF = CRF(BVOC_{2100}) - CRF(BVOC_{2000})$

$\Delta CSDRF = CSDRF(BVOC_{2100}) - CSDRF(BVOC_{2000})$.

Subscripts "2000" and "2100" denotes that BVOC emissions from this year were used, while other model conditions were based on present-day values.

3. Results

3.1 Present-day expanse of larch forest and BVOC emissions

LPJ-GUESS reproduces the present-day circumpolar permafrost distribution (Figure 1; shown as circumpolar map for comparison with Tarnocai et al (2009)) and, with the exception of the Kamchatka peninsula, simulates also the expanse of the larch-dominated forests in Eastern Siberia (Figure 1; Miller and Smith, 2012, Wagner, 1997). Maximum leaf area index (LAI) calculated by the model for the Spasskaya Pad forest (62°15'18.4"N, 129°37'07.9"E, 220 m a.s.l), where the BVOC measurements were obtained, was 2.0 (averaged over years 1981-2000; not shown), and is in good agreement with the measured values during that period (1.6; Takeshi et al., 2008). Total present-day modelled soil C pools over the top 2 m in Eastern Siberia are 216 Gt C, and 454 Gt C for circumpolar soils summed for latitudes above 40°N (Table 2). A recent estimate of C stored in northern latitude soils affected by permafrost was 191, 495, and 1024 Gt C in the 0-30, 0-100 and 0-300 cm soil layer, based on extrapolating observations stored in the Northern Circumpolar Soil Carbon Database (Tarnocai et al., 2009). These numbers indicate that the values calculated with LPJ-GUESS are lower than observation-based ones, most likely underestimating C-density in particular in the soil layers below few tenths of cm.

Kajos et al. (2013) measured for the first time *MT E** from *L. cajanderii*. Their measurements, taken over an entire growing season at Spasskaya Pad, suggested values of E^* ranging from 1.9 μg C m^{-2}(leaf) h^{-1} at the lower end, to 9.6 μg C m^{-2}(leaf) h^{-1} at the upper. Applying a weighted measured-average E^* of 6.2 μg C m^{-2}

(leaf) h^{-1} , in LPJ-GUESS led to average summer daily monoterpene emissions of 2.9 (± 0.8, 1 standard deviation, June) mg C m^{-2} d^{-1}, and 2.2 (± 0.8, July) mg C m^{-2} d^{-1} for the gridlocation representing the Spasskaya Pad site, and for the same year of measurements than reported in Kajos et al (2013). These values are within 25 and 10% of measured values (3.3 ± 2.9 mg C m^{-2} d^{-1}, June; 2.4 ± 1.6 mg C m^{-2} d^{-1}; July), even though the modelled day-to-day variation was smaller which is expected when applying grid-averaged climate as model input. By comparison, for a boreal Scots pine forest in southern Finland average June and July monoterpene emissions were somewhat larger than the values for larch (3.8 and 5.1 mg C m^{-2} d^{-1}, respectively; Rantala *et al.*, 2015). For a Larix kaempferi-dominated temperate forest in Japan, Mochizuki et al (2012) extrapolated, based on their measurements, summer time maxima of ca. 10 mg C m^{-2} d^{-1} .Across the Siberian larch biome applying E^* of 6.2 μg C m^{-2} increased simulated total present-day *MT* emissions from 0.11 $TgCa^{-1}$ (as in Schurgers et al., 2009a) to 0.21 $TgCa^{-1}$, or to 0.42 $TgCa^{-1}$ when the maximum E^* was used (Table 2). The observed range in E^*, and the calculated range in total emissions across Siberia, might reflect variability in tree microclimate or genetic variability, or might have been induced by (undetected) mechanic or biotic stress during the time of measurements (Staudt et al., 2001; Bäck et al., 2012; Kajos et al., 2013). While our data are insufficient to make a finite suggestion of *L. cajanderi* E^*, the measurements provide evidence for potentially substantially higher *MT* emissions from Siberian larch than previous estimates.

3.2 Present-day aerosols, and links to BVOC

New particle formation events (Figure 2a) were observed regularly at Spasskaya Pad. The calculated volumetric source rates of condensing vapours (*Q*), the product of vapour concentration required for the observed particle growth rate and particle loss rate (Kulmala et al., 2005), increased exponentially with temperature (Figure 2b). *MT* concentrations increased with temperature as well, with a slope relatively similar to that found for the *Q vs*. T relationship (Figure 2c). Consequently, a positive relationship emerged between *Q* and *MT* concentration (Figure 2d), which supports previous field and laboratory evidence that *MT* and their oxidation products are a main precursor to the observed particle formation and growth.

Figure 2d shows the connection between the BVOC concentration and the formation rate of vapours causing the growth of the aerosol particles. Even though the monoterpene concentrations were measured above and the aerosol growth rates below the canopy, the observed correlation indicates that BVOC concentration is an important contributor to the regional aerosol growth and supports the theory that the condensation of organic vapour is largely responsible for the formation of secondary organic aerosol (Hallquist et al., 2009, Carslaw et al., 2010). Substantial within-canopy chemical reactions would be expected to worsen the relationship. The correlation depicted in Figure 2d is determined in particular by the the formation of secondary organic aerosol on pre-existing aerosol particles, whereas the nucleation rate of new aerosol particles seems not to be dominated by the landscape-scale emissions and surface concentrations of BVOCs. For instance, most nucleation events in a Scots pine dominated landscape in Finland have been found in spring, when measured monoterpene concentrations in the near-surface were about one tenth of the summer time maximum (ca. 60 ppt, *vs*. up to 500 ppt; Haapanala et al., 2007; Lappalainen et al., 2009). We found here MT concentrations of similar magnitude to these.

By contrast to temperature and BVOC concentrations, levels of radiation, which can be considered a surrogate for the concentration of the OH radical (OH•), did not affect *Q* (Figure 2b), even though OH• has been considered an important player for aerosol formation. Rohrer and Berresheim (2006) showed a strong correlation between solar ultraviolet radiation and OH• concentration at the Hohenpeissenberg site in Germany. Furthermore, Hens et al. (2014) demonstrated that the day-time OH• concentrations in (especially) boreal forest depend on solar radiation, both above and below the canopy. Hence, the poor relation between the source rate of condensing vapour and orders-of-magnitude variation in levels of radiation (Fig. 2b) indicates that OH-radical concentration did not have a major impact on Q. This agrees with the findings by Ehn et al. (2014) that ozone instead of OH• is an important, if not the main, atmospheric agent oxidising organic vapours into a chemical form that condenses on particle surfaces. Since the relative variation in ozone concentrations is much smaller than in BVOC (or OH) concentrations (Hens et al., 2014), the similarity in the dependencies of Q and MT concentration and temperature (Figures 2b and 2c) are in favour of a more significant role of ozone than of OH in the formation of condensable vapours. In general, our results indicate that factors and processes besides the concentrations of SO_2 and OH• seem to limit aerosol production in non-polluted environments (Kulmala et al., 2005).

3.3 Future carbon pools, vegetation distribution and BVOC emissions in Siberia

In a warmer environment with higher atmospheric CO_2 levels, the simulations indicated drastically reduced area of permafrost in Siberia (Figure 1). Total net primary productivity in the simulated domain increased from an annual average of 3.5 PgC a^{-1} to 5.9 PgC a^{-1} at the end of the 21st century. An overall C loss of 100 PgC assumed to be in the form of CO_2 (since the model does not yet include a dynamic surface hydrology which would be necessary to assess changing methane emissions) at the end of the 21st century, compared to present-day conditions, was calculated from the shrinking Siberian areas of permafrost (Table 2). However, warming and higher levels of atmospheric CO_2 led also to increasing LAI, and to larch-dominated areas showing the expected north- and north-eastwards shift (Figure 1) compared to present-day climate (Miller and Smith, 2012). The carbon uptake in expanding vegetation into permafrost-free areas, combined with enhanced productivity across the simulation domain overcompensates for the losses from C-pools in permafrost areas (Table 2).

Without CO_2 inhibition of BVOC emissions future *MT* emissions were, as expected, notably enhanced: directly as a result of warmer leaves, but augmented by the future higher LAI of larch and evergreen conifers (Figure 1D; Table 2, Figure A1). Since the emissions scale with the emission factors applied, the proportional increase between present-day and future climate conditions is independent of the value of *E**. Whether or not leaf *MT* emissions are inhibited by increasing atmospheric CO_2 levels to similar degree to what was found for isoprene is difficult to assess from today's limited number of studies (e.g., Niinemets et al., (2010), and references therein). We included both simulation results in Table 2 since similarities in the leaf metabolic pathways of isoprene and *MT* production suggest such an inhibition, but possibly this effect does not become apparent in plant species where produced *MT* are stored unless the storage pools become measurably depleted by the reduced production. By contrast, species emitting *MT* in an "isoprene-like" fashion immediately after production should more directly reflect CO_2 inhibition. Evergreen conifers typically emit most *MT* from

storage pools, although recent experiments have shown that some light-dependent emissions also contribute to total emission fluxes. Accordingly, based on the leaf-level measurements, larch could follow a hybrid pattern between emission after production and from storage (Kajos et al., 2013). Without accounting for CO_2 inhibition, *MT* emissions across the model domain more than doubled (Figure 1; Table 2) by 2100, as a consequence of higher emissions per leaf area due to warmer temperatures, and of the larger emitting leaf area in response to higher photosynthesis. With CO_2 inhibition included, simulated changes were negligible, similar to what was shown in previous BVOC simulations with the model (Arneth et al.,2007a; Arneth et al., 2008).

4. Discussion

Boreal vegetation has been shown to respond to the recent decades' warming and increasing atmospheric CO_2 levels with a prolonged growing season and higher maximum LAI, similar to patterns in our simulations (Piao et al., 2006). The calculated enhanced biomass growth is in-line with experimental evidence of higher C in plant biomass in warming plots at tundra field sites (Elmendorf et al., 2012;Sistla et al., 2013). In Siberian mountain regions, an upward movement of vegetation zones has been recorded already (Soja et al., 2007), while the analysis of evergreen coniferous undergrowth abundance and age shows spread of evergreen species, especially *Pinus siberia*, into Siberian larch forest (Kharuk et al., 2007). These observations thus support the modelled shift in vegetation zones, and change in vegetation type composition and productivity. Likewise, other models with dynamic vegetation also have shown a strong expansion of broadleaved forests at the southern edge of the Siberian region in response to warming (Shuman et al., 2015).

Warming and thawing of permafrost soils is being observed at global monitoring network sites, including in Russia (Romanovsky et al., 2010). Estimates of carbon losses from northern wetland and permafrost soils in response to 21st century warming range from a few tens to a few hundreds Pg C, depending on whether processes linked to microbial heat production, thermokarst formation and surface hydrology, winter snow cover insulation, dynamic vegetation, C-N interactions, or fire are considered (Khvorostyanov et al., 2008;Schuur et al., 2009; Arneth et al., 2010; Koven et al., 2011; Schneider von Deimling et al., 2012). For instance, a modelled range of 0.07 - 0.23 Wm^{-2} forcing associated with a 33 - 114 $PgCO_2$-C loss from permafrost regions was found for a simulation study that was based on the RCP 8.5 climate and CO_2 scenarios, but excluding full treatment of vegetation dynamics (Schneider von Deimling et al., 2012). In a recent literature review, Schaefer et al (2014) found a range from cumulative 46 to 435 CO_2 –equivalents (accounting for CO_2 and CH_4), or 120 ± 85 GtC by 2100 in response to different future warming scenarios and modelling approaches. In our simulation, the CO_2-C loss from the decreasing Siberian permafrost region would be equivalent to a 0.13 additional Wm^{-2} forcing in 2100 (see methods). Likely, this number is too low since the model does not include thermokarst processes, which can facilitate rapid thaw (Schaefer et al., 2014, and references therein). The modelled carbon loss was offset when taking into account vegetation dynamics and processes across the entire Siberian study-domain (Table 2), including a shift in PFT composition, and enhanced productivity especially in the southern regions, such that the overall carbon uptake including enhanced net primary productivity and expanding woody vegetation resulted in a small negative (-0.09 Wm^{-2}) effect.

LPJ-GUESS is a second generation DGVM (Fisher et al., 2010) and includes plant demography, such that forest successional dynamics and competition for water and light between individual age-cohorts are treated explicitly (Smith et al., 2001). The forest growth dynamics thus differentiate between early successional, short-lived species that invest in rapid growth and shade-tolerant trees with resource allocation aimed towards longer-lived growth strategies. As a result, the model's PFTs can be mapped to tree-species when required information for model parameterisation is available. The process-based treatment of resource competition such as for light and water has been shown to lead to a realistic growth response and distribution under present-day climate condition (Arneth et al., 1998; Schurgers er al., 2009b), which should also hold in future and past climates (Miller et al., 2008; Schurgers et al., 2009b). This feature also provides a distinct advantage when applying the necessary BVOC emission capacities that are based on species (rather than functional-type) average values (Arneth et al., 2008; Schurgers et al., 2009b; Niinemets et al., 2010). In earlier simulations (Schurgers et al., 2009a), a generic emission potential of E^*= 2.4 μg C m^{-2}(leaf) h^{-1} was adopted for the BNS PFT based on a recommendation in Guenther et al., (1995), that at that time did not include observations from any larch species. Here we demonstrate not only that a range of measured larch E^* (see Table 2) introduces large uncertainty in total MT emissions from Siberia, but also that it is fundamental to apply dynamic vegetation growth response (rather than static maps) for BVOC emissions estimates in changing environments.

Monoterpene compounds can be emitted either directly following their synthesis in the chloroplast, in an "isoprene-like" fashion, or from storage pools, resulting in an emission pattern that is independent of light availability. The observed emissions of monoterpenes by larch possibly reflect a hybrid pattern between emission directly after synthesis in the chloroplast and emission from storage pools, as has also been found for other coniferous species (Schurgers et al., 2009a). The needle-level measurements by Kajos et al. (2013) on larch indicated a combined light- and temperature response, even though a robust differentiation to a temperature-only model was not possible due to the limited sample size. An earlier study by Ruuskanen et al. (2007) on a 5-year old *L. sibirica* tree indicated a better performance of the temperature-only emission model for monoterpene species compared to the light and temperature approach.

Multiple interacting processes can alter monoterpene emissions in future. Irrespective of the relative roles of light *vs*. temperature dependence, a change in *MT* concentrations and hence partial pressure of *MT* in stored pools, for instance in response to long-term warming, would affect emission capacities. Changes in measured E^* when investigated over the course of a growing season have been reported and could be related to a changing production rate (Niinemets et al., 2010). Likewise, observed profiles of E^* within tree canopies appear not only related to changes in leaf area-to-weight ratios along the canopy light and temperature gradients, but also to varying production rates (Niinemets et al., 2010). Emission capacities in *Q. ilex* leaves adapted to warm growth environment were notably enhanced (Staudt et al., 2003), but the experimental basis for an acclimation response of BVOC emissions to temperature remains remarkably poor (Penuelas and Staudt, 2010) and is indicative of the general lack of global modelling studies accounting for possibly acclimation of process responses to environmental changes (Arneth et al., 2012). In our simulations we aim to provide a range

399 of a possible plastic BVOC-CO_2 response by switching the direct CO_2 inhibition on and off for both isoprene
400 and monoterpene, but we do not account for other acclimation processes.
401 The assessment of climate effects of changes in the CO_2-C balance *vs* those of BVOC-SOA interactions is
402 challenging, since the translation of regional changes in emissions of atmospherically reactive species into
403 related radiative forcing and then into a response in the climate system is highly non-linear and poorly
404 understood (Shindell et al., 2008; Fiore et al., 2012). Based on a synthesis of measured aerosol number
405 concentrations and size distribution combined with boundary layer growth modelling Paasonen et al. (2013)
406 estimated a growing-season indirect radiative cloud albedo feedback of -0.5 $Wm^{-2}K^{-1}$ for the Siberian larch
407 region. The observation-based indirect feedback factors exceeded direct ones by roughly an order of magnitude
408 (Paasonen et al., 2013), but a simple extrapolation based on the region's growing season temperature increases
409 of *c.* 5.5 K simulated at the end of the 21st century in our study with the ECHAM GCM does not account for
410 the important non-linearities in the system. Present-day CCN (1.0%) concentration over Siberia was estimated
411 to vary from extremely low values of less than 50 cm^{-3} north of 60ºN to a few hundred per cc in the southern
412 part of Siberian domain (Figure 3). In order to put measurements and model simulations into context, simulated
413 CCN concentrations (at the Spasskaya Pad location) were evaluated against observations during May-August,
414 using particle diameter (dp) >100nm as proxy for CCN, since CCN at different supersaturations was
415 unavailable in the observations. The model reproduces the observed May-August average CCN concentration
416 (dp>100 nm) and CCN maximum location in July (not shown), but the seasonal variation was overestimated
417 in the simulations. ECHAM-HAM indicates a transition from very clean spring aerosol population of ~100
418 cm^{-3} to high July concentrations ranging from 800 to 1200 cm^{-3} in the Yakutsk region. By contrast, observations
419 show only moderate monthly CCN variability from 550 cm^{-3} in May to 750 cm^{-3} in July. While the simulated
420 low spring concentrations likely reflect unaccounted-for anthropogenic emissions, the simulated high summer
421 concentrations result from strong wildfire emissions in the region in the applied emission inventory (see
422 below).
423 Whether or not BVOCs can increase the availability of CCN depends on the availability of sub-CCN sized
424 particles (O'Donnell et al., 2011). In the future, a scenario of decreasing anthropogenic emissions led to a
425 strong decrease in calculated atmospheric SO_2 concentrations and also of particle nucleation (Makkonen et al.,
426 2012a). In the model experiments anthropogenic primary emissions are introduced as 60 nm particles, hence
427 condensation of sulfuric acid and organic vapours is generally needed in order to grow these particles to CCN
428 sizes. However, the modelled primary particle emissions are dominated by wildfires, which are assumed to
429 inject large particles with 150 nm diameter. SOA formation only partly enhances the survival of small particles
430 by providing additional growth (Makkonen et al., 2012a), but partly also suppresses it by increasing the
431 coagulation sink for small particles (Figure A2, lower left panel; see also O'Donnell et al., 2011).
432 The assumption of unchanging oxidant fields induces some uncertainty for future simulations and
433 inconsistency with present-day simulations with varying biogenic emissions, since both anthropogenic and
434 biogenic emissions are likely to modify the atmospheric oxidative capacity. Nudging towards reanalysis
435 meteorology establishes evaluation of BVOC-aerosol coupling with unchanged meteorological fields, but
436 restricts the model in terms of aerosol-climate feedbacks, since e.g., nudging future climate simulations with

present-day meteorological winds is based on the assumption that e.g. or wind direction and –speed etc. are not changing.

When only BVOC emissions were changed between present day and levels simulated for climate in 2100, the relatively higher emission of BVOC leads to substantially increased aerosol growth rates (GR) over a large part of the Siberian domain. This was the case even though we chose the conservative estimate based on the low measured E^* of 1.9 μg C m^{-2} h^{-1}. However, GR is not the only factor determining levels of CCN. Increased aerosol mass due to increased SOA formation led also to an increase in the condensation sink and eventually to even decreased particle formation rates in some regions (Figure A2, lower right panel). These competing effects of increased growth and increased sink are essential for quantifying the importance of the cloud albedo forcing feedback. We can also show that the patterns of changes in CCN in response to future BVOC emissions are additionally affected by changes in the aerosol background, which strongly influences the indirect aerosol effect of SOA. In large parts of Siberia, the simulated BVOC oxidation products condense on CCN-sized aerosols already present from wildfires When simulation results were separated into regions of low and high wildfire emissions (Figure 4) areas of low wildfire activity had relatively large increase in SOA formation (60%) in nucleation mode (d_p<10 nm). The relative increases in SOA formation in Aitken, accumulation and coarse modes were 50%, 31% and 40%, respectively. However, the distribution of BVOC oxidation products was rather different in areas of high wildfire activity: the condensation of SOA depends on surface area and organic mass of the population, both of which are shifted towards larger modes in wildfire-intensive areas. SOA formation in coarse mode was more than doubled, while SOA in nucleation mode decreased by 30% due to decrease in nucleation rates and increase in vapour sink in large aerosol modes. It is clear that the effect of increased BVOC emission on particle population has distinct effects depending on existing background aerosol distribution. Moreover, CCN at 1.0% supersaturation was used, even though "realistic" supersaturations are generally lower. The CCN(1.0%) concentration therefore provide a upper limit for CCN concentration. In the aerosol model, neither the simulated CCN(1.0%) nor e.g., CCN(0.2%) correspond clearly to either Aitken or accumulation modes. CCN at 0.2% would reflect larger aerosols, and hence the changes in CCN(0.2%) would be less sensitive to aerosol and precursor sources (see corresponding Figure A3).

Averaged over Siberian areas of low wildfire activity, the median (mean) increase of CCN(0.2%) was calculated to be 1% (7%) due to BVOC emissions changes from present-day levels to the end of the 21st century, while areas of high wildfire emission lead to median (mean) increase of 0.3% (0.5%).

Even though the Siberian *MT* emissions more than double until 2100 (Table 2), the increasing wildfire emissions and decreasing new particle formation due to reductions in anthropogenic SO_2 largely offset the effect of increased BVOC emissions on CCN concentration. In wildfire plumes, the simulated CCN concentrations were high even without BVOC-induced growth of smaller particles. The radiative effect due to BVOC emission change between *ca*. 2000 and *ca*. 2100 was estimated from ECHAM-HAM simulations averaged over 5 years. The increase in BVOC emission leading to additional secondary organic aerosol induces a -0.2 W m^{-2} change in direct clear-sky aerosol forcing over the Siberian domain at the end of the 21st century. Furthermore, the increase in CCN concentrations leads to a strengthening of the cloud radiative effect by -0.5 W m^{-2} (Table 3). These changes in radiative fluxes only take into account the changing BVOC emission, and

475 the potential concurrent changes in anthropogenic and wildfire emissions might decrease the simulated
476 radiative effect of biogenic SOA (Carslaw et al., 2013).
477
478 **5. Implications, limitations and future progress**
479 Up to now, studies that investigate the role of terrestrial vegetation dynamics and carbon cycle in the
480 climate system typically account solely for CO_2, while studies that look at BVOC-climate interactions often
481 ignore other processes, especially interactions with vegetation dynamics or the CO_2- balance of ecosystems.
482 However, for understanding the full range of interactions between atmospheric composition, climate change
483 and terrestrial processes we need a much more integrative perspective. Our analysis seeks to provide an
484 example of how to quantify a number of climatically relevant ecosystem processes in the large Eastern Siberian
485 region in a consistent observational and modelling framework that accounts for the multiple interactions
486 between emissions, vegetation and soils. It poses a challenge to combine effects of well mixed greenhouse
487 gases and locally constrained, short-lived substances. On global-scale level, the opposing estimates in radiative
488 effects from ecosystem-CO_2 and -BVOC-SOA interactions are miniscule but it is to be expected that some of
489 the forcing effects from SOA could lead to a notable change in regional temperatures. Clearly, our numbers
490 are uncertain but they pinpoint the necessity for assessing surface-atmosphere exchange processes
491 comprehensively in climate feedback analyses. While doing so, we are aware of the fact that a number of
492 additional processes are not included in our analysis. For instance, it remains to be investigated whether a
493 similar picture would emerge when additional feedback mechanisms are taken into consideration, e.g. SOA
494 formation from isoprene (Henze and Seinfeld, 2006) or effects of atmospheric water vapour on reaction rates
495 and aerosol loads, or that some of the SOA might like to partition more to the gas-phase in a warmer climate.
496 Likewise, neither the albedo effect of northwards migrating vegetation (Betts, 2000; Zhang et al., 2014),
497 changes in the hydrology (which affects CH_4 and N_2O vs. CO_2 fluxes), nor changes in C-N interactions (Zaehle
498 et al., 2010) are considered here, which would require a coupled ESM that combines a broad range of
499 dynamically varying ecosystem processes with full treatment of air chemistry and aerosol interactions.
500 Quantifying the full range of terrestrial climate feedbacks, either globally or regionally, with consistent model
501 frameworks that account for the manifold interactions is not yet possible with today's modelling tools.
502
503
504
505 **Acknowledgements**
506 AA acknowledges support from Swedish Research Council VR, and the Helmholtz Association
507 ATMO Programme, and its Initiative and Networking Fund. The study was also supported by the
508 Finnish Academy, grant 132100. The EU FP7 Bacchus project (grant agreement 603445) is
509 acknowledged for financial support. PM acknowledges support from the VR Linnaeus Centre of
510 Excellence LUCCI, RM Makkonen acknowledges support from the Nordic Centre of Excellence
511 CRAICC. This study is a contribution to the Strategic Research Area MERGE.
512

513 **References**

514 Ahlström, A., Schurgers, G., Arneth, A., and Smith, B.: Robustness and uncertainty in terrestrial
515 ecosystem carbon response to cmip5 climate change projections, Environmental Research Letters, 7, 044008,
516 doi: 10.1088/1748-9326/7/4/044008 2012.
517
518 Arneth, A., Miller, P. A., Scholze, M., Hickler, T., Schurgers, G., Smith, B., and Prentice, I. C.: CO_2
519 inhibition of global terrestrial isoprene emissions: Potential implications for atmospheric chemistry,
520 Geophysical Research Letters, 34, L18813, doi: 10.1029/2007GL030615, 2007a.
521
522 Arneth, A., Niinemets, U., Pressley, S., Back, J., Hari, P., Karl, T., Noe, S., Prentice, I. C., Serca, D.,
523 Hickler, T., Wolf, A., and Smith, B.: Process-based estimates of terrestrial ecosystem isoprene emissions:
524 incorporating the effects of a direct CO_2-isoprene interaction, Atmospheric Chemistry and Physics, 7, 31-53,
525 2007b.
526 Arneth, A., Schurgers, G., Hickler, T., and Miller, P. A.: Effects of species composition, land surface
527 cover, CO_2 concentration and climate on isoprene emissions from European forests, Plant Biol., 10, 150-162,
528 doi:10.1055/s-2007-965247, 2008.
529 Arneth, A., Harrison, S. P., Zaehle, S., Tsigaridis, K., Menon, S., Bartlein, P. J., Feichter, J., Korhola, A.,
530 Kulmala, M., O'Donnell, D., Schurgers, G., Sorvari, S., and Vesala, T.: Terrestrial biogeochemical feedbacks
531 in the climate system, Nature Geosci, 3, 525-532, doi: 10.1038/ngeo1905, 2010.
532 Arneth, A., Schurgers, G., Lathiere, J., Duhl, T., Beerling, D. J., Hewitt, C. N., Martin, M., and Guenther,
533 A.: Global terrestrial isoprene emission models: sensitivity to variability in climate and vegetation, Atmos.
534 Chem. Phys., 11, 8037-8052, 10.5194/acp-11-8037-2011, 2011.
535 Arneth, A., Mercado, L., Kattge, J., and Booth, B. B. B.: Future challenges of representing land-processes
536 in studies on land-atmosphere interactions, Biogeosciences, 9, 3587-3599, 10.5194/bg-9-3587-2012, 2012.
537 Betts, R. A.: Offset of the potential carbon sink from boreal forestation by decreases in surface albedo,
538 Nature, 408, 187-190, 2000.Bäck, J., Aalto, J., Henriksson, M., Hakola, H., He, Q., and Boy, M.:
539 Chemodiversity of a scots pine stand and implications for terpene air concentrations, Biogeosciences, 9,
540 689-702, 10.5194/bg-9-689-2012, 2012.
541 Carslaw, K. S., Boucher, O., Spracklen, D. V., Mann, G. W., Rae, J. G. L., Woodward, S., and Kulmala,
542 M.: A review of natural aerosol interactions and feedbacks within the earth system, Atmospheric Chemistry
543 and Physics, 10, 1701-1737, 2010.
544 Carslaw, K. S., Lee, L. A., Reddington, C. L., Pringle, K. J., Rap, A., Forster, P. M., Mann, G. W.,
545 Spracklen, D. V., Woodhouse, M. T., Regayre, L. A., and Pierce, J. R.: Large contribution of natural aerosols
546 to uncertainty in indirect forcing, Nature, 503, 67-71, 10.1038/nature12674, 2013.
547 Dentener, F., Kinne, S., Bond, T., Boucher, O., Cofala, J., Generoso, S., Ginoux, P., Gong, S.,
548 Hoelzemann, J. J., Ito, A., Marelli, L., Penner, J. E., Putaud, J. P., Textor, C., Schulz, M., van der Werf, G.
549 R., and Wilson, J.: Emissions of primary aerosol and precursor gases in the years 2000 and 1750 prescribed
550 data-sets for AeroCom, Atmos. Chem. Phys., 6, 4321-4344, 2006.
551 Dolman, A. J., Maximov, T. C., Moors, E. J., Maximov, A. P., Elbers, J. A., Kononov, A. V., Waterloo,
552 M. J., and van der Molen, M. K.: Net ecosystem exchange of carbon dioxide and water of far eastern
553 Siberian Larch (Larix cajanderii) on permafrost, Biogeosciences, 1, 133-146, 2004.
554 Ehn, M., Thornton, J. A., Kleist, E., Sipila, M., Junninen, H., Pullinen, I., Springer, M., Rubach, F.,
555 Tillmann, R., Lee, B., Lopez-Hilfiker, F., Andres, S., Acir, I. H., Rissanen, M., Jokinen, T., Schobesberger,
556 S., Kangasluoma, J., Kontkanen, J., Nieminen, T., Kurten, T., Nielsen, L. B., Jorgensen, S., Kjaergaard, H.
557 G., Canagaratna, M., Dal Maso, M., Berndt, T., Petaja, T., Wahner, A., Kerminen, V. M., Kulmala, M.,
558 Worsnop, D. R., Wildt, J., and Mentel, T. F.: A large source of low-volatility secondary organic aerosol,
559 Nature, 506, 476-479, doi: 10.1038/nature13032, 2014.
560 Elmendorf, S. C., Henry, G. H. R., Hollister, R. D., Bjork, R. G., Boulanger-Lapointe, N., Cooper, E. J.,
561 Cornelissen, J. H. C., Day, T. A., Dorrepaal, E., Elumeeva, T. G., Gill, M., Gould, W. A., Harte, J., Hik, D.
562 S., Hofgaard, A., Johnson, D. R., Johnstone, J. F., Jonsdottir, I. S., Jorgenson, J. C., Klanderud, K., Klein, J.
563 A., Koh, S., Kudo, G., Lara, M., Levesque, E., Magnusson, B., May, J. L., Mercado-Diaz, J. A., Michelsen,
564 A., Molau, U., Myers-Smith, I. H., Oberbauer, S. F., Onipchenko, V. G., Rixen, C., Schmidt, N. M., Shaver,
565 G. R., Spasojevic, M. J., Porhallsdottir, P. E., Tolvanen, A., Troxler, T., Tweedie, C. E., Villareal, S.,
566 Wahren, C. H., Walker, X., Webber, P. J., Welker, J. M., and Wipf, S.: Plot-scale evidence of tundra

vegetation change and links to recent summer warming, Nat. Clim. Chang., 2, 453-457, doi: 10.1038/nclimate1465, 2012.

Fisher, R., McDowell, N., Purves, D., Moorcroft, P., Sitch, S., Cox, P., Huntingford, C., Meir, P., and Woodward, F. I.: Assessing uncertainties in a second-generation dynamic vegetation model caused by ecological scale limitations, New Phytologist, 187, 666-681, 10.1111/j.1469-8137.2010.03340.x, 2010

Fiore, A. M., Naik, V., Spracklen, D. V., Steiner, A., Unger, N., Prather, M., Bergmann, D., Cameron-Smith, P. J., Cionni, I., Collins, W. J., Dalsoren, S., Eyring, V., Folberth, G. A., Ginoux, P., Horowitz, L. W., Josse, B., Lamarque, J.-F., MacKenzie, I. A., Nagashima, T., O'Connor, F. M., Righi, M., Rumbold, S. T., Shindell, D. T., Skeie, R. B., Sudo, K., Szopa, S., Takemura, T., and Zeng, G.: Global air quality and climate, Chemical Society Reviews, 41, 6663-6683, doi: 10.1039/c2cs35095e, 2012.

Guenther, A., Hewitt, C. N., Erickson, D., Fall, R., Geron, C., Graedel, T., Harley, P., Klinger, L., Lerdau, M., McKay, W. A., Pierce, T., Scholes, B., Steinbrecher, R., Tallamraju, R., Taylor, J., and Zimmermann, P.: A global model of natural volatile organic compound emissions, Journal of Geophysical Research, 100, 8873-8892, 1995.

Haapanala, S., Ekberg, A., Hakola, H., Tarvainen, V., Rinne, J., Hellen, H., and Arneth, A.: Mountain birch - potentially large source of sesquiterpenes into high latitude atmosphere, Biogeosciences, 6, 2709-2718, 2009.

Hallquist, M., Wenger, J. C., Baltensperger, U., Rudich, Y., Simpson, D., Claeys, M., Dommen, J., Donahue, N. M., George, C., Goldstein, A. H., Hamilton, J. F., Herrmann, H., Hoffmann, T., Iinuma, Y., Jang, M., Jenkin, M. E., Jimenez, J. L., Kiendler-Scharr, A., Maenhaut, W., McFiggans, G., Mentel, T. F., Monod, A., Seinfeld, J. H., Surratt, J. D., Szmigielski, R., and Wildt, J.: The formation, properties and impact of secondary organic aerosol: Current and emerging issues, Atmos. Chem. Phys., 9, 5155-5235, 2009.

Hakola, H., Tarvainen, V., Back, J., Ranta, H., Bonn, B., Rinne, J., and Kulmala, M.: Seasonal variation of mono- and sesquiterpene emission rates of Scots pine, Biogeosciences, 3, 93-101, 2006.

Hens, K., Novelli, A., Martinez, M., Auld, J., Axinte, R., Bohn, B., Fischer, H., Keronen, P., Kubistin, D., Nölscher, A. C., Oswald, R., Paasonen, P., Petäjä, T., Regelin, E., Sander, R., Sinha, V., Sipilä, M., Taraborrelli, D., Tatum Ernest, C., Williams, J., Lelieveld, J., and Harder, H.: Observation and modelling of HO_x radicals in a boreal forest, Atmos. Chem. Phys., 14, 8723-8747, doi:10.5194/acp-14-8723-2014, 2014.

Henze, D., and Seinfeld, J. H.: Global secondary organic aerosol from isoprene oxidation, Geophysical Research Letters, 33, L09812, doi: 10.1029/2006GL025976, 2006.

Hickler, T., Vohland, K., Feehan, J., Miller, P. A., Smith, B., Costa, L., Giesecke, T., Fronzek, S., Carter, T. R., Cramer, W., Kuhn, I., and Sykes, M. T.: Projecting the future distribution of European potential natural vegetation zones with a generalized, tree species-based dynamic vegetation model, Global Ecology and Biogeography, 21, 50-63, doi: 10.1111/j.1466-8238.2010.00613.x, 2012.

Holst, T., Arneth, A., Hayward, S., Ekberg, A., Mastepanov, M., Jackowicz-Korczynski, M., Friborg, T., and Crill, P. M.: Bvoc ecosystem flux measurements at a high latitude wetland site, Atmospheric Chemistry and Physics, 10, 1617-1634, 2010.

Hussein, T., Dal Maso, M., Petäjä, T., Koponen, I. K., Paatero, P., Aalto, P. P., Hämeri, K., and Kulmala, M.: Evaluation of an automatic algorithm for fitting the particle number size distributions Boreal Environment Research, 10, 337-355, 2005.

IPCC: Climate Change 2007: The Physical Science Basis. Summary for Policymakers. Contribution of Working Group I to the Fourth Assessment Report of the Intergovernmental Panel on Climate Change, Cambridge University Press, Cambridge, 2007.

Jokinen, T., Berndt, T., Makkonen, T., Kerminen, V.-M., Junninen, H., Paasonen, P., Stratmann, F., Herrmann, H., Guenther, A., Worsnop, D. R., Kulmala, M., Ehn, M., and Sipilä, M.: Production of extremely low-volatile organic compounds from biogenic emissions: Measured yields and atmospheric implications, Proceedings of the National Academy of Sciences of the United States of America, doi:10.1073/pnas.1423977112, 2015.

Kajos, M. K., Hakola, H., Holst, T., Nieminen, T., Tarvainen, V., Maximov, T., Petäjä, T., Arneth, A., and Rinne, J.: Terpenoid emissions from fully grown East Siberian *Larix cajanderi* trees, Biogeosciences, 10, 4705-4719, doi: 10.5194/bg-10-4705-2013, 2013.

Kharuk, V., Ranson, k., and Dvinskaya, M.: Evidence of Evergreen Conifer Invasion into Larch Dominated Forests During Recent Decades in Central Siberia, Eurasian Journal of Forest Research, 10, 163-171, 2007.

Khvorostyanov, D. V., Ciais, P., Krinner, G., and Zimov, S. A.: Vulnerability of east Siberia's frozen carbon stores to future warming, Geophys. Res. Lett., 35, L10703, doi:10710.1029/2008GL033639, 2008.

Kobak, K. I., Turchinovich, I. Y., Kondrasheva, N. Y., Schulze, E. D., Schulze, W., Koch, H., and Vygodskaya, N. N.: Vulnerability and adaptation of the larch forest in eastern Siberia to climate change, Water, Air, & Soil Pollution, 92, 119-127, 1996.

Koven, C. D., Ringeval, B., Friedlingstein, P., Ciais, P., Cadule, P., Khvorostyanov, D., Krinner, G., and Tarnocai, C.: Permafrost carbon-climate feedbacks accelerate global warming, Proceedings of the National Academy of Sciences of the United States of America, 108, 14769-14774, doi: 10.1073/pnas.1103910108, 2011.

Kulmala, M., Dal Maso, M., Makela, J. M., Pirjola, L., Vakeva, M., Aalto, P., Miikkulainen, P., Hameri, K., and O'Dowd, C. D.: On the formation, growth and composition of nucleation mode particles, Tellus Ser. B-Chem. Phys. Meteorol., 53, 479-490, doi: 10.1034/j.1600-0889.2001.530411.x, 2001.

Kulmala, M., Petäjä, T., Mönkkönen, P., Koponen, I. K., Dal Maso, M., Aalto, P., Lehtinen, K. E. J., and Kerminen, V. M.: On the growth of nucleation mode particles: source rates of condensable vapor in polluted and clean environments, Atmospheric Chemistry and Physics, 4, 409-416, 2005.

Lappalainen, H. K., Sevanto, S., Back, J., Ruuskanen, T. M., Kolari, P., Taipale, R., Rinne, J., Kulmala, M., and Hari, P.: Day-time concentrations of biogenic volatile organic compounds in a boreal forest canopy and their relation to environmental and biological factors, Atmospheric Chemistry and Physics, 9, 5447-5459, 2009.

Makkonen, R., Asmi, A., Kerminen, V. M., Boy, M., Arneth, A., Guenther, A., and Kulmala, M.: BVOC-aerosol-climate interactions in the global aerosol-climate model ECHAM5.5-HAM2, Atmos. Chem. Phys., 12, 10077-10096, 10.5194/acp-12-10077-2012, 2012a.

Makkonen, R., Asmi, A., Kerminen, V. M., Boy, M., Arneth, A., Hari, P., and Kulmala, M.: Air pollution control and decreasing new particle formation lead to strong climate warming, Atmos. Chem. Phys., 12, 1515-1525, doi: 10.5195/acp-1515-2012, 2012b.

Miller, P. A., Giesecke, T. T. Hickler, R. H. W. Bradshaw, B. Smith, H. Seppä, P. J. Valdes, M. T. Sykes. Exploring climatic and biotic controls on Holocene vegetation change in Fennoscandia, Journal of Ecology 96(2), 247-259, 10.1111/j.1365-2745.2007.01342.x, 2008

Miller, P. A., and Smith, B.: Modelling tundra vegetation response to recent arctic warming, Ambio, 41, 281-291, doi: 10.1007/s13280-12-306-1, 2012.

Mitchell, T. D., and Jones, P. D.: An improved method of constructing a database of monthly climate observations and associated high-resolution grids, International Journal of Climatology, 25, 693-712, 2005.

Mochizuki, T., Tani, A., Takahashi, Y., Saigusa, N., Ueyama, M., 2014. Long-term measurement of terpenoid flux above a Larix kaempferi forest using a relaxed eddy accumulation method. Atmospheric Environment 83, 53-61.

Moser, L., Fonti, p., Büntgen, U., Esper, J., Luterbacher, J., Franzen, J., and Frank, D.: Timing and duration of European larch growing season along altitudinal gradients in the Swiss Alps, Tree Physiology, 30, 225-233. doi:10.1093/treephys/tpp108, 2012.

Nieminen, T., Lehtinen, K. E. J., and Kulmala, M.: Sub-10 nm particle growth by vapor condensation – effects of vapor molecule size and particle thermal speed, Atmos. Chem. Phys., 10, 9773-9779, doi: 10.5194/acp-10-9773-2010, 2010.

Nieminen, T., Asmi, A., Dal Maso, M., Aalto, P. P., Keronen, P., Petaja, T., Kulmala, M., and Kerminen, V.-M.: Trends in atmospheric new-particle formation: 16 years of observations in a boreal-forest environment, Boreal Environment Research, 19, 191-214, 2014.

Niinemets, U., Tenhunen, J. D., Harley, P. C., and Steinbrecher, R.: A model of isoprene emission based on energetic requirements for isoprene synthesis and leaf photosynthetic properties for *Liquidambar* and *Quercus*, Plant, Cell and Environment, 22, 1319-1335, 1999.

Niinemets, Ü., Monson, R. K., Arneth, A., Ciccioli, P., Kesselmeier, J., Kuhn, U., Noe, S. M., Penuelas, J., and Staudt, M.: The emission factor of volatile isoprenoids: caveats, model algorithms, response shapes and scaling, Biogeosciences, 7, 1809-1832, SRef-ID: 1726-4189/bg/2010-7-1809, 2010.

O'Donnell, D., Tsigaridis, K., and Feichter, J.: Estimating the direct and indirect effects of secondary organic aerosols using ECHAM5-HAM, Atmos. Chem. Phys., 11, 8635-8659, doi: 10.5194/acp-11-8635-2011, 2011.

Ohta, T., Hiyama, T., Tanaka, H., Kuwada, T., Maximov, T. C., Ohata, T., and Fukushima, Y.: Seasonal variation in the energy and water exchanges above and below a larch forest in eastern Siberia, Hydrological Processes, 15, 1459-1476, 2001.

Paasonen, P., Asmi, A., Petaja, T., Kajos, M. K., Aijala, M., Junninen, H., Holst, T., Abbatt, J. P. D., Arneth, A., Birmili, W., van der Gon, H. D., Hamed, A., Hoffer, A., Laakso, L., Laaksonen, A., Richard Leaitch, W., Plass-Dulmer, C., Pryor, S. C., Raisanen, P., Swietlicki, E., Wiedensohler, A., Worsnop, D. R., Kerminen, V.-M., and Kulmala, M.: Warming-induced increase in aerosol number concentration likely to moderate climate change, Nature Geosci, 6, 438-442, doi: 10.1038/ngeo1800, 2013.

Penuelas, J., and Staudt, M.: Bvocs and global change, Trends in Plant Science, 15, 133-144, 10.1016/j.tplants.2009.12.005, 2010.

Piao, S., Friedlingstein, P., Ciais, P., Zhou, L., and Chen, A.: Effect of climate and CO_2 changes on the greening of the Northern Hemisphere over the past two decades, Geophys. Res. Lett., 33, L23402, doi: 10.1029/2006gl028205, 2006.

Rantala, P., Aalto, J., Taipale, R., Ruuskanen, T.M., Rinne, J., 2015. Annual cycle of volatile organic compound exchange between a boreal pine forest and the atmosphere. Biogeosciences 12, 5753-5770.

Riahi, K., Gruebler, A., and Nakicenovic, N.: Scenarios of long-term socio-economic and environmental development under climate stabilization, Technol. Forecast. Soc. Change, 74, 887-935, 2007.

Rohrer, F. and Berresheim, H.: Strong correlation between levels of tropospheric hydroxyl radicals and solar ultraviolet radiation, Nature, 442, 184–187, 2006.

Romanovsky, V. E., Drozdov, D. S., Oberman, N. G., Malkova, G. V., Kholodov, A. L., Marchenko, S. S., Moskalenko, N. G., Sergeev, D. O., Ukraintseva, N. G., Abramov, A. A., Gilichinsky, D. A., and Vasiliev, A. A.: Thermal state of permafrost in russia, Permafrost and Periglacial Processes, 21, 136-155, 10.1002/ppp.683, 2010.Ruuskanen, T. M., Kajos, M. K., Hellén, H., Hakola, H., Tarvainen, V., and Rinne, J.: Volatile organic compound emissions from Siberian larch, Atmospheric Environment, 41, doi:10.1016/j.atmosenv.2007.05.036 2007.

Schaefer, K., Lantuit, H., Romanovsky, V. E., Schuur, E. A. G., and Witt, R.: The impact of the permafrost carbon feedback on global climate, Environmental Research Letters, 9, 085003, 10.1088/1748-9326/9/8/085003, 2014.

Schneider von Deimling, T., Meinshausen, M., Levermann, A., Huber, V., Frieler, K., Lawrence, D. M., and Brovkin, V.: Estimating the near-surface permafrost-carbon feedback on global warming, Biogeosciences, 9, 649-665, doi: 10.5194/bg-9-649-2012, 2012.

Schurgers, G., Arneth, A., Holzinger, R., and Goldstein, A. H.: Process-based modelling of biogenic monoterpene emissions: sensitivity to temperature and light, Atmospheric Chemistry and Physics, 9, 3409-3423, 2009a.

Schurgers, G., Hickler, T., Miller, P. A., and Arneth, A.: European emissions of isoprene and monoterpenes from the Last Glacial Maximum to present, Biogeosciences, 6, 2779-2797, 2009b.

Schuur, E. A. G., Vogel, J. G., Crummer, K. G., Lee, H., Sickman, J. O., and Osterkamp, T. E.: The effect of permafrost thaw on old carbon release and net carbon exchange from tundra, Nature, 459, 556-559, doi: 10.1038/nature08031, 2009.

Serreze, M. C., Walsh, J. E., Chapin, F. S., Osterkamp, T., Dyurgerov, M., Romanovsky, V., Oechel, W. C., Morison, J., Zhang , T., and Barry, R. G.: Observational evidence of recent change in the northern high-latitude environment, Climatc Change, 46, 159-207, 2000.

Shindell, D. T., Levy, H., Schwarzkopf, M. D., Horowitz, L. W., Lamarque, J. F., and Faluvegi, G.: Multimodel projections of climate change from short-lived emissions due to human activities, Journal of Geophysical Research-Atmospheres, 113, doi:10.1029/2007JD009152, D11109, 2008.

Shuman, J. K., Tchebakova, N. M., Parfenova, E. I., Soja, A. J., Shugart, H. H., Ershov, D., and Holcomb, K.: Forest forecasting with vegetation models across russia, Canadian Journal of Forest Research, 45, 175-184, 10.1139/cjfr-2014-0138, 2015

Sistla, S. A., Moore, J. C., Simpson, R. T., Gough, L., Shaver, G. R., and Schimel, J. P.: Long-term warming restructures Arctic tundra without changing net soil carbon storage, Nature, 497, 615-618, doi: 10.1038/nature12129, 2013.

Sitch, S., Smith, B., Prentice, I. C., Arneth, A., Bondeau, A., Cramer, W., Kaplan, J. O., Levis, S., Lucht, W., Sykes, M. T., Thonicke, K., and Venevsky, S.: Evaluation of ecosystem dynamics, plant geography and terrestrial carbon cycling in the LPJ dynamic global vegetation model, Glob. Change Biol., 9, 161-185, 2003.

Sitch, S., Cox, P. M., Collins, W. J., and Huntingford, C.: Indirect radiative forcing of climate change through ozone effects on the land-carbon sink, Nature, 448 (7155), 791-794, doi:10.1038/nature06059, 2007.

Smith, B., Prentice, I. C., and Sykes, M. T.: Representation of vegetation dynamics in the modelling of terrestrial ecosystems: comparing two contrasting approaches within European climate space, Global Ecology & Biogeography, 10, 621-637, 2001.

Soja, A. J., Tchebakova, N. M., French, N. H. F., Flannigan, M. D., Shugart, H. H., Stocks, B. J., Sukhinin, A. I., Parfenova, E. I., Chapin Iii, F. S., and Stackhouse, J. P. W.: Climate-induced boreal forest change: Predictions versus current observations, Global and Planetary Change, 56, 274-296, doi: 10.1016/j.gloplacha.2006.07.028, 2007.

Spracklen, D. V., Bonn, B., and Carslaw, K.: Boreal forests, aerosols and the impacts on clouds and climate, Philosophical Transactions of the Royal Society of London Series A, 366, 4613–4626, doi: 10.1098/rsta.2008.0201, 2008a.

Spracklen, D. V., Carslaw, K. S., Kulmala, M., Kerminen, V.-M., Sihto, S.-L., Riipinen, I., Merikanto, J., Mann, G. W., Chipperfield, M. P., Wiedensohler, A., Birmili, W., and Lihavainen, H.: Contribution of particle formation to global cloud condensation nuclei concentrations, Geophysical Research Letters, 35, L06808, doi: 10.01029/2007GL033038, 2008b.Staudt, M., Mandl, N., Joffre, R., and Rambal, S.: Intraspecific variability of monoterpene composition emitted by quercus ilex leaves, Canadian Journal of Forest Research, 31, 174-180, 10.1139/x00-153, 2001.

Staudt, M., Joffre, R., and Rambal, S.: How growth conditions affect the capacity of *quercus ilex* leaves to emit monoterpenes, New Phytologist, 158, 61-73, 2003.

Stier, P., Feichter, J., Kinne, S., Kloster, S., Vignati, E., Wilson, J., Ganzeveld, L., Tegen, I., Werner, M., Balkanski, Y., Schulz, M., and Bouche, O.: The aerosol-climate model Echam5-Ham, Atmospheric Chemistry and Physics, 5, 11125-11156, 2005.

Svenningsson, B., Arneth, A., Hayward, S., Holst, T., Massling, A., Swietlicki, E., Hirsikko, A., Junninen, H., Riipinen, I., Vana, M., dal Maso, M., Hussein, T., and Kulmala, A. E.: Aerosol particle formation events and analysis of high growth rates observed above a subarctic wetland–forest mosaic, Tellus B, 58, 353-364, doi: 10.1111/j.1600-0889.2008.00351.x, 2008.

Takeshi, O., Maximov, T. C., Dolman, A. J., Nakai, T., van der Molen, M. K., Kononov, A. V., Maximov, A. P., Hiyama, T., Iijima, Y., Moors, E. J., Tanaka, H., Toba, T., and Yabuki, H..: Interannual variation of water balance and summer evapotranspiration in an eastern Siberian larch forest over a 7-year period (1998–2006), Agricultural and Forest Meteorology, 48, 1940-1953, 2008.

Tarnocai, C., Canadell, J. G., Schuur, E. A. G., Kuhry, P., Mazhitova, G., and Zimov, S.: Soil organic carbon pools in the northern circumpolar permafrost region, Global Biogeochemical Cycles, 23, Gb2023, doi: 10.1029/2008gb003327, 2009.

Tchebakova, N. M., Rehfeldt, G. E., and Parfenova, E. I.: Impacts of climate change on the distribution of *Larix spp.* and *Pinus sylvestris* and their climatypes in Siberia, Mitigation and Adaptation Strategies for Global Change, 11, 861-882, doi: 10.1007/s11027-005-9019-0, 2006.

Thonicke, K., Venevsky, S., Sitch, S., and Cramer, W.: The role of fire disturbance for global vegetation dynamics. Coupling fire into a Dynamic Global Vegetation Model, Global Ecology & Biogeography, 10, 661-678, 2001.

Tunved, P., Hansson, H. C., Kerminen, V. M., Strom, J., Maso, M. D., Lihavainen, H., Viisanen, Y., Aalto, P. P., Komppula, M., and Kulmala, M.: High natural aerosol loading over boreal forests, Science, 312, 261-263, doi: 10.1126/science.1123052, 2006.

Tsigaridis, K., Daskalakis, N., Kanakidou, M., Adams, P. J., Artaxo, P., Bahadur, R., Balkanski, Y., Bauer, S. E., Bellouin, N., Benedetti, A., Bergman, T., Berntsen, T. K., Beukes, J. P., Bian, H., Carslaw, K. S., Chin, M., Curci, G., Diehl, T., Easter, R. C., Ghan, S. J., Gong, S. L., Hodzic, A., Hoyle, C. R., Iversen, T., Jathar, S., Jimenez, J. L., Kaiser, J. W., Kirkevåg, A., Koch, D., Kokkola, H., Lee, Y. H, Lin, G., Liu, X., Luo, G., Ma, X., Mann, G. W., Mihalopoulos, N., Morcrette, J.-J., Müller, J.-F., Myhre, G., Myriokefalitakis, S., Ng, N. L., O'Donnell, D., Penner, J. E., Pozzoli, L., Pringle, K. J., Russell, L. M., Schulz, M., Sciare, J., Seland, Ø., Shindell, D. T., Sillman, S., Skeie, R. B., Spracklen, D., Stavrakou, T., Steenrod, S. D., Takemura, T., Tiitta, P., Tilmes, S., Tost, H., van Noije, T., van Zyl, P. G., von Salzen, K., Yu, F., Wang, Z., Wang, Z., Zaveri, R. A., Zhang, H., Zhang, K., Zhang, Q., and Zhang, X.: The AeroCom evaluation and intercomparison of organic aerosol in global models, Atmos. Chem. Phys., 14, 10845-10895, doi:10.5194/acp-14-10845-2014, 2014.

Vignati, E., Wilson, J., and Stier, P.: M7: An efficient size-resolved aerosol microphysics module for large-scale aerosol transport models, Journal of Geophysical Research, 109, D22202, doi:10.1029/2003JD004485, 2004.

Wagner, V.: Analysis of a Russian landscape map and landscape classification for use in computer-aided forestry research, International Institute for Applied Systems Analysis, Laxenburg, 1997.

Wania, R., Ross, I., and Prentice, I. C.: Integrating peatlands and permafrost into a dynamic global vegetation model: I. Evaluation and sensitivity of physical land surface processes, Global Biogeochemical Cycles 23, GB3014, doi:10.1029/2008GB003412, 2009.

Zhang, K., O'Donnell, D., Kazil, J., Stier, P., Kinne, S., Lohmann, U., Ferrachat, S., Croft, B., Quaas, J., Wan, H., Rast, S., and Feichter, J.: The global aerosol-climate model ECHAM-HAM, version 2: sensitivity to improvements in process representations, Atmospheric Chemistry and Physics, 12, 8911–8949, doi:10.5194/acp-8912-8911-2012, 2012.

Zhang, W., Jansson, C., Miller, P. A., Smith, B., and Samuelsson, P.: Biogeophysical feedbacks enhance the arctic terrestrial carbon sink in regional earth system dynamics, Biogeosciences, 11, 5503-5519, 10.5194/bg-11-5503-2014, 2014.

Zhang, K., Wan, H., Liu, X., Ghan, S. J., Kooperman, G. J., Ma, P.-L., Rasch, P. J., Neubauer, D., and Lohmann, U.: Technical note: On the use of nudging for aerosol–climate model intercomparison studies, Atmos. Chem. Phys., 14, 8631-8645, doi:10.5194/acp-14-8631-2014, 2014.

Zaehle, S., Friedlingstein, P., and Friend, A. D.: Terrestrial nitrogen feedbacks may accelerate future climate change, Geophysical Research Letters, 37, L01401, doi: 10.01029/02009GL041345 2010.

804 Table 1: Overview over modelled processes, and model-specific features. For further details see text.

Process	Model	Input	Input source	Resolution	Configuration	Specific features
BVOC emissions	LPJ-GUESS, dynamic global vegetation model	Air temperature, precipitation, short-wave radiation (monthly, interpolated to daily), atmospheric CO2 levels (annual).	ECHAM historical (20th century) and RCP 8.5 (21st century), interpolated to CRU climate, following Ahlström et al. (2012)	0.5 X 0.5 degrees horizontal	As in Arneth et al. (2007a) and Schurgerst et al. (2009b)	BNS plant functional type adopted for larch-specific parameters (see text). Inhibition of BVOC emissions by atmospheric CO_2 can be switched on and off.
Ecosystem dynamics and carbon cycle	As above	As above	As above	As above	As in Miller and Smith, 2012	Including permafrost module
Aerosol number concentration and size distribution: black carbon, organic carbon, dust, sea salt and sulfate	ECHAM5.5-HAM2, Global climate model coupled with aerosol microphysics	Emissions of BVOC, from wildfire, anthropogenic sources, dust and seasalt	Climate generated as part of simulation nudged to ERA-40; BVOC from LPJ-GUESS; as in Makkonen et al., (2012); dust/seasalt modelled interactively, anthropogenic and wildfire emissions fixed to present day (Stier et al., 2005; Makkonen et al., (2012)	T63 spectral resolution, 31 vertical hybrid sigma levels	As in Makkonen et al. (2012)	SOA module includes formation of extremely low volatility organic compounds from MT oxidation (Jokinen et al. 2015)
Total particle and cloud concentration nuclei concentration, radiative effects	As above	As above	As above	As above	As in Lohmann et al., 2007	Aerosol concentrations are interactively coupled to the cloud-microphysics scheme, calculation of aerosol direct and indirect effect

805

Table 2: Simulated changes in net primary productivity, BVOC emissions, and C pool size in vegetation and soils. Unless stated otherwise, values are for the simulated Siberian domain (76-164°E, 46-71°N), and represent an area of 1.2 E^7 km^2. NPP_{global} (given as a reference value) is global vegetation net primary productivity (Pg C a^{-1}). BVOC in Tg C a^{-1}, CO_2-C fluxes in Pg C a^{-1}, C pools in PgC.

Simulations for monoterpene emissions for the boreal needleleaf summergreen (BNS) plant functional type compared three cases (indicated as different subscripts for "Total_MT_{BNS}"): using maximum (9.6 μgC g^{-1} h^{-1}) and minimum (1.9 μgC g^{-1} h^{-1}) values for E^* measured in Spasskaya Pad (see text), and $E^* = 6.2 \mu g_C$ g^{-1} h^{-1} as a weighted average from all observations at the Spasskaya Pad location. For BVOC, CO_2 inhibition was switched on and off (Arneth et al., 2007b).

	1981-2000	2031-2050	2081-2100
NPP_{global}	58 ± 15	66 ± 17	76 ± 14
NPP	3.5 ± 0.2	4.5 ± 0.2	5.9 ± 0.2
Carbon in circumpolar permafrost region:			
Vegetation	109 ± 0.7	106 ± 1.6	78 ± 1.8
Litter	81 ± 0.5	68 ± 0.3	44 ± 0.3
Soil (0 to 2 m depth)	454 ±0.03	392 ± 0.4	255 ± 0.5
Total	644 ± 0.4	567 ± 1.1	377 ± 1.0
C-pools in permafrost area of study domain			
Vegetation	41 ± 0.6	38 ± 0.6	35 ± 0.7
Litter	40 ± 0.3	34 ± 0.2	23 ± 0.2
Soil (0 to 2 m depth)	216 ± 0.06	187 ± 0.1	140 ± 0.3
Total	297 ± 0.4	259 ± 0.4	198 ± 0.2
C-pools in entire Siberian study domain:			
Vegetation	45 ± 0.5	56 ± 1.5	77 ± 2.8
Litter	41 ± 0.5	43 ± 0.3	41 ± 0.7
Soil (0 to 2 m depth)	219 ± 0.3	221 ± 0.3	223 ± 0.3
Total	305 ± 1.1	320 ± 2.1	342 ± 2.0
BVOC, with CO_2 inhibition:			
Total_iso	4.11 ± 0.29	4.52 ± 0.32	4.80 ± 0.24
BNE, MT	1.03 ± 0.07	1.06 ± 0.06	1.02 ± 0.04
BINE, MT	0.23 ± 0.01	0.23 ± 0.01	0.18 ± 0.01
BNS, MT_1.9	0.09 ± 0.01	0.10 ± 0.02	0.09 ± 0.01
BNS, MT_6.2	0.28 ± 0.04	0.33 ± 0.06	0.29 ± 0.04
BNS, MT_9.6	0.43 ± 0.06	0.52 ± 0.09	0.45 ± 0.06
Total_$MT_{BNS_1.9}$	1.40 ± 0.09	1.44 ± 0.10	1.33 ± 0.06
Total_ $MT_{BNS\_6.2}$	1.60 ± 0.11	1.68 ± 0.14	1.53 ± 0.88
Total_ $MT_{BNS\ \_9.6}$	1.75 ± 0.12	1.86 ± 0.16	1.69 ± 0.10
BVOC, no CO_2 inhibition:			
Total_iso	3.9 ± 0.29	6.0 ± 0.48	11.0 ± 1.06
BNE, MT	0.99 ± 0.07	1.41 ± 0.1	2.33 ± 0.19
BINE, MT	0.22 ± 0.01	0.30 ± 0.02	0.42 ± 0.02
BNS, MT_1.9	0.08 ± 0.01	0.14 ± 0.02	0.20 ± 0.03
BNS, MT_6.2	0.21±0.03	0.35±0.06	0.52±0.07
BNS, MT_9.6	0.42±0.06	0.69±0.11	1.02±0.13

Total_$MT_{BNS_1.9}$	1.34±0.09	1.92±0.13	3.04±0.23
Total_ $MT_{BNS\_6.2}$	1.47±0.10	2.13±0.16	3.36±0.27
Total_ $MT_{BNS\_9.6}$	1.67±0.13	2.47±0.22	4.90±0.47

Abbreviations:
NPP: net primary productivity;
BNE: boreal needleleaf evergreen PFT, shade tolerant;
BINE: boreal needleleaf evergreen PFT, intermediate shade-tolerant;
BNS: boreal needleleaf summergreen PFT ("larch"), shade intolerant, continentality index as in Sitch et al., (2003);
Iso: isoprene;
MT, monoterpenes.

Table 3: Simulated changes in radiative effects due to change in BVOC emission between years 2000 and 2100, averaged over Siberian domain, Northern Hemisphere and globally. CRF: cloud radiative forcing; CSDRF, direct aerosol effect that accounts only for clear-sky short-wave forcing.

	ΔCRF (Wm^{-2})	ΔCSDRF (Wm^{-2})
Siberia	-0.50	-0.21
Northern hemisphere	-0.30	-0.01
Global	-0.03	-0.01

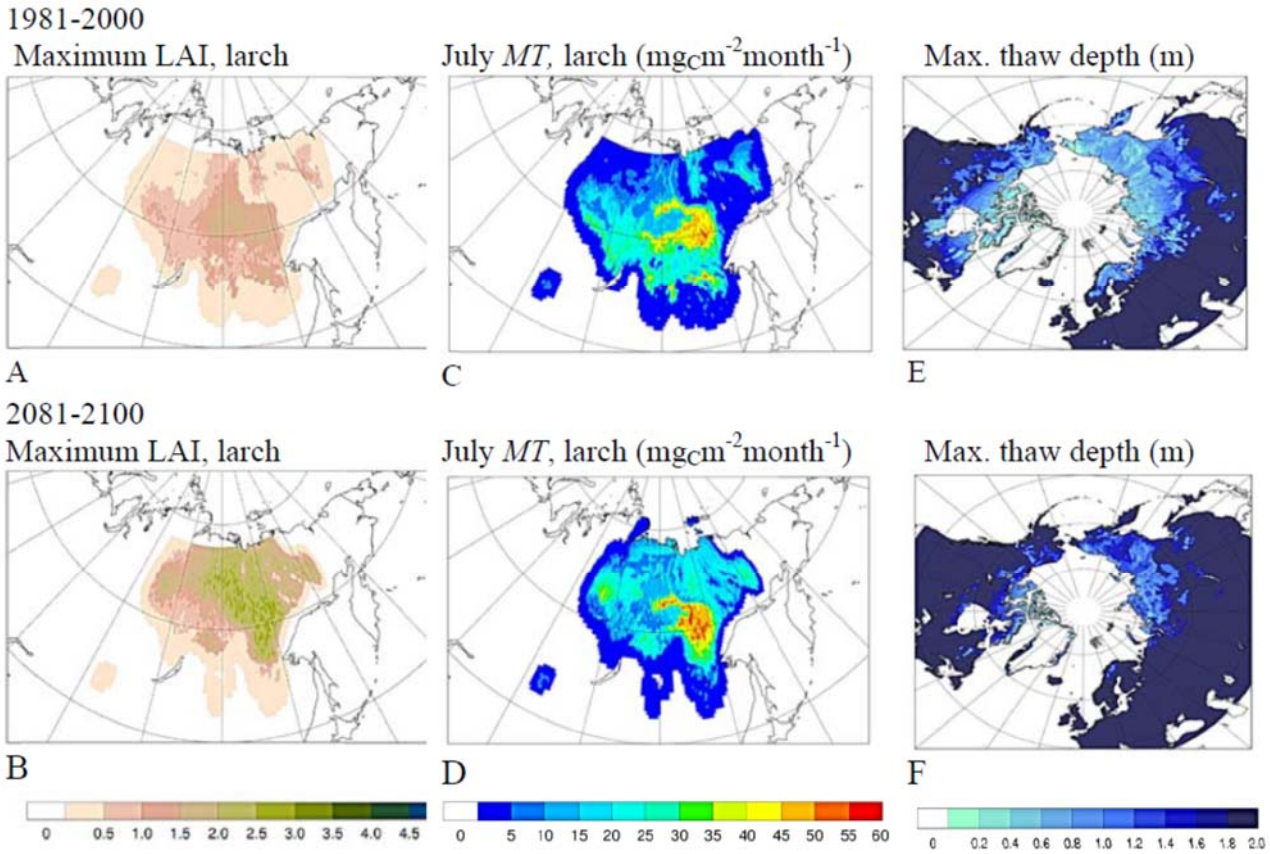

Figure 1: Simulated maximum summer monthly leaf area index (LAI; A, B) and July emissions of monoterpenes (C, D; mgC m^{-2} $month^{-1}$) from Eastern Siberian larch. The latter were calculated applying emission factors of 6.2**,** obtained from the measurements at Spasskaya Pad. Panels E and F: maximum permafrost thaw depth (August), shown here as the circumpolar map for comparison with Tarnocai et al. (Tarnocai et al., 2009). Values are averages for a simulation 1981-2000 (panels A, C, E), and for 2081-2100 (panels B, D, F), applying climate and CO_2 concentrations from ECHAM-RCP8.5. Emissions in panel C, D do not account for direct CO_2 inhibition (see also Figure A1).

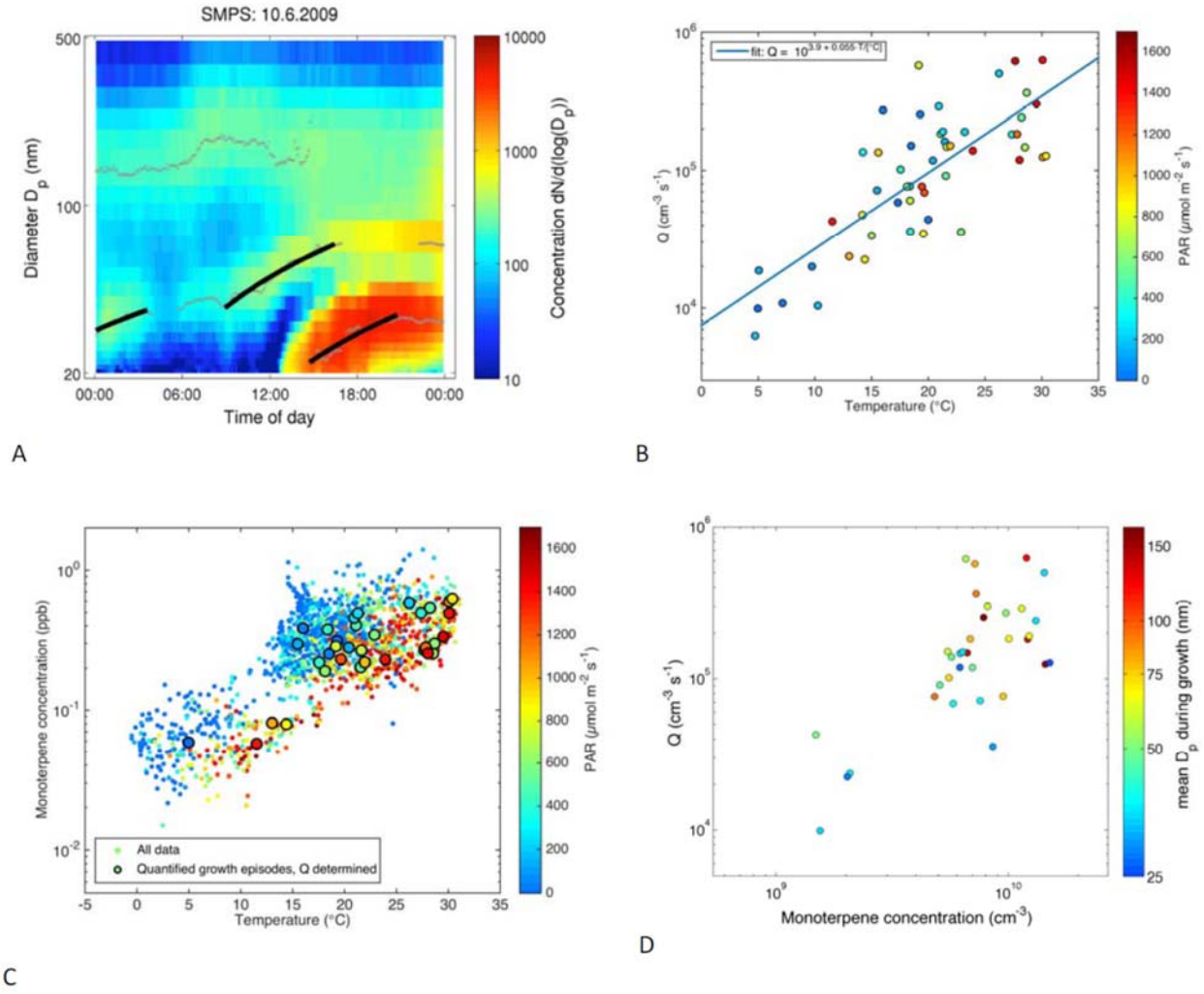

Figure 2: Particle growth rates obtained from particle number size distribution (panel A, example from day 10.6.2009). The colours indicate the measured concentrations (d*N*/d log*Dp*, cm^{-3}) of particles with different diameters (D_p, nm) over the course of a day, small circles are mean diameters of concentration modes fitted for each measurement, and the temporal change of these diameters is represented with black lines from which the growth rate is calculated. Panel B shows the calculated volumetric source rates of condensing vapours (Q, molecules cm^{-3} s^{-1}; 10-minute resolution) as a function of air temperature (°C) for all identified growth periods (one data point is obtained for each fitted growth rate, e.g. from panel A three data points would have been extracted); data are separated by levels of photosynthetically active radiation (PAR). Panel C: Monoterpene concentrations (half hourly data) measured above the canopy *vs.* temperature measured at the same level (data separated by PAR, the data points overlapping with determined growth rate in panel B are indicated by encircled symbols). , and relationship between volumetric source rate of condensing vapours and monoterpene concentration (D; data separated by particle diameter). Data points in panel (D) correspond directly to encircled symbols in panel B.

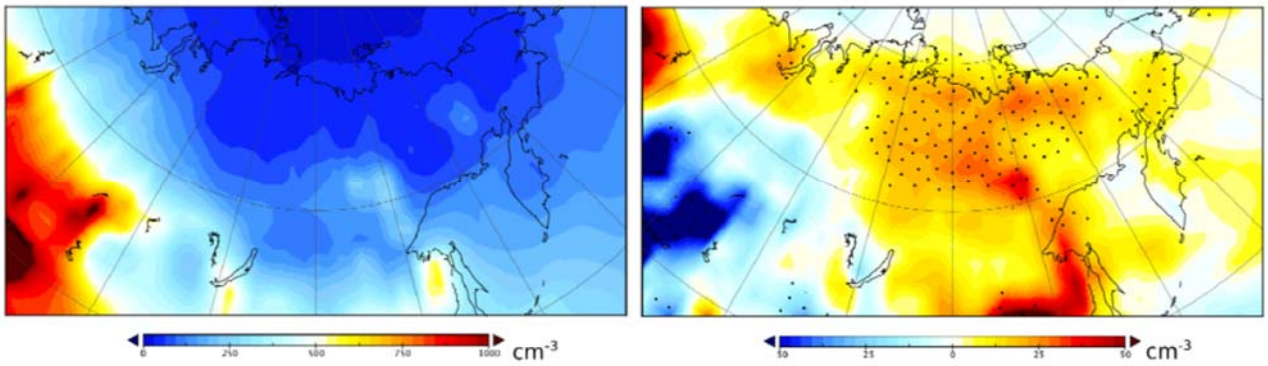

Figure 3. Annual average boundary-layer CCN (1.0%) concentration (cm^{-3}) in Siberia with present-day anthropogenic and BVOC (for BNS: E*=1.9) emissions (left panel), and changes in CCN (1.0%; right panel) concentration due to increase in BVOC emission between years 2000 and 2100 (simulations with CO_2 inhibition off). Areas with statistical significant changes in CCN are indicated by dots. The statistical analysis is based on monthly average CCN concentrations from 5-years of simulated data, and statistical significance of the CCN anomaly is evaluated using a two-sample t test, without assuming equal variance between the two populations.

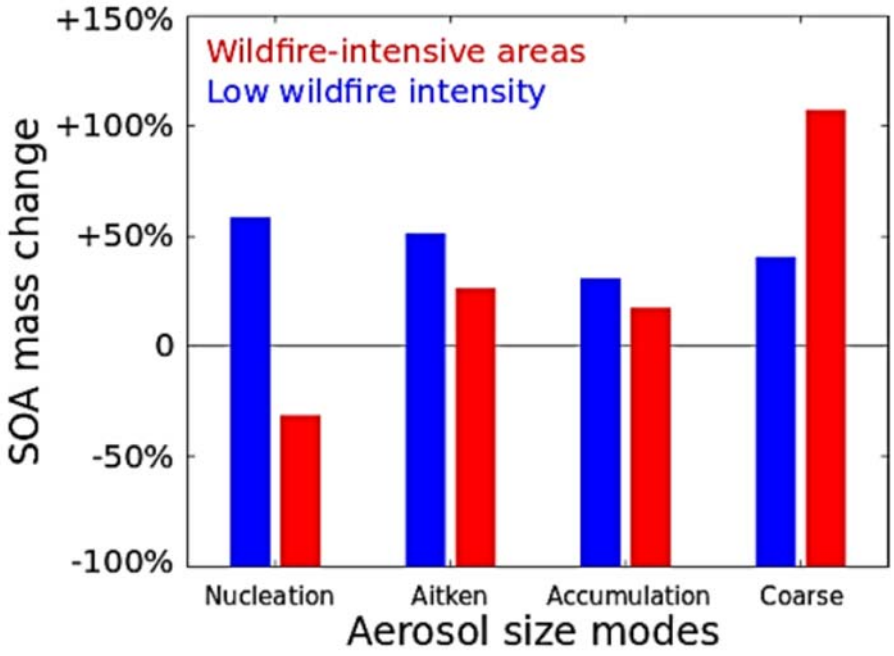

Figure 4. Relative increase in SOA mass, simulated by ECHAM5-HAM in different aerosol size modes due to BVOC emissions increase from the year 2000 to 2100. The areas are averaged over Siberia, and the BVOC emissions for years 2000 to 2100 (example is for = E^* 1.9). Areas were separated by wildfire emissions (using an emission limit of 10^{-11} kg m^{-2} s^{-1}). In the Siberian domain, accumulation mode includes over 85% of organic aerosol, and the absolute changes in SOA are also dominated by accumulation mode. However, the SOA condensation increase until year 2100 is essential for nucleation and Aitken mode growth.

Appendix:

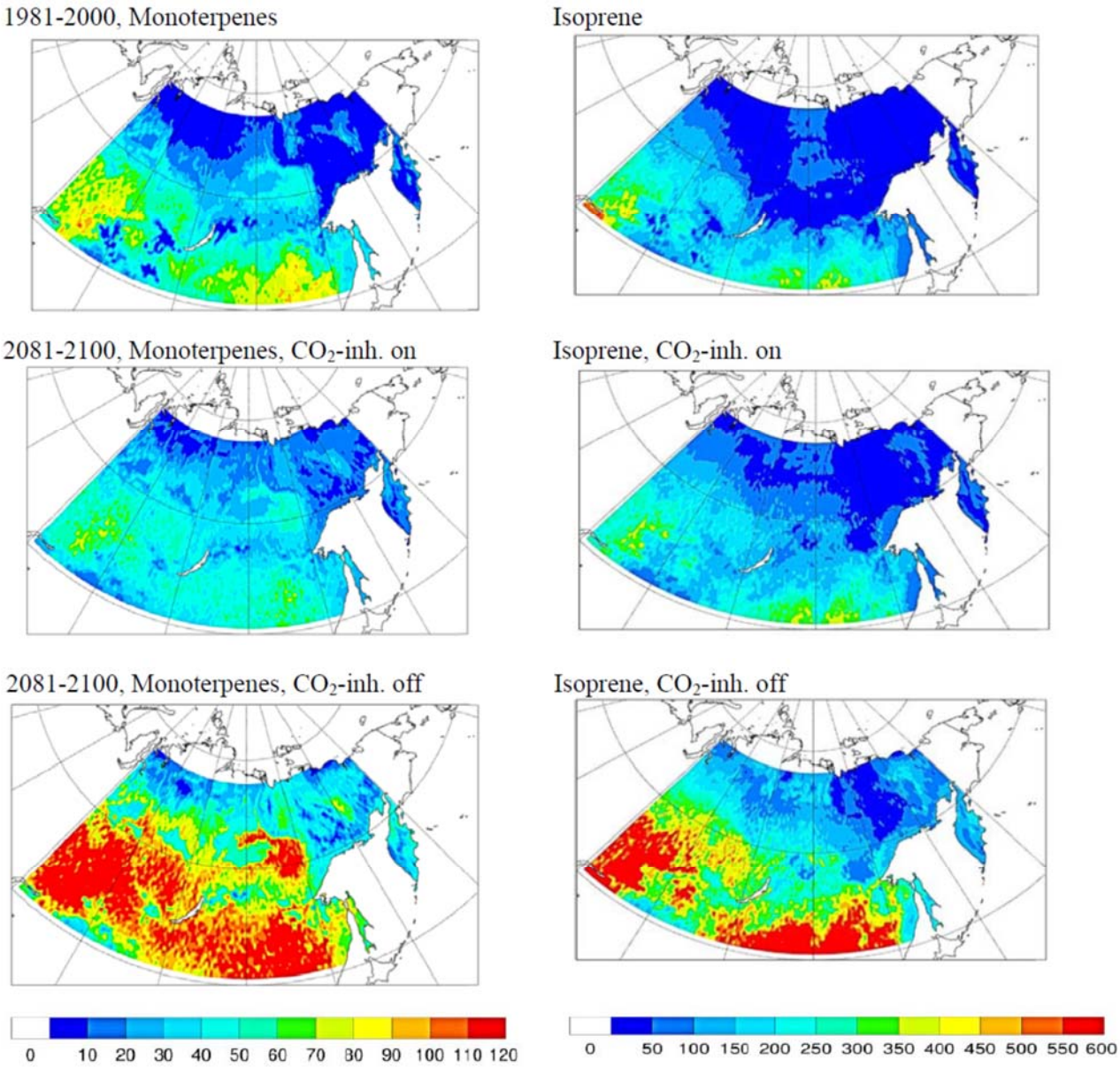

Figure A1: Present-day (top: 1981-2000) and end of 21st century (bottom: 2081-2100) total monoterpene (left) and isoprene (right) emissions for the month July ($mg_C\ m^{-2}\ month^{-1}$). Future simulations show results with CO_2 inhibition switched on and off; for present-day conditions the CO_2-effect on BVOC is marginal as the values are close to the standardised concentration of 370ppm, and therefore only the patterns without CO_2-effect is shown.

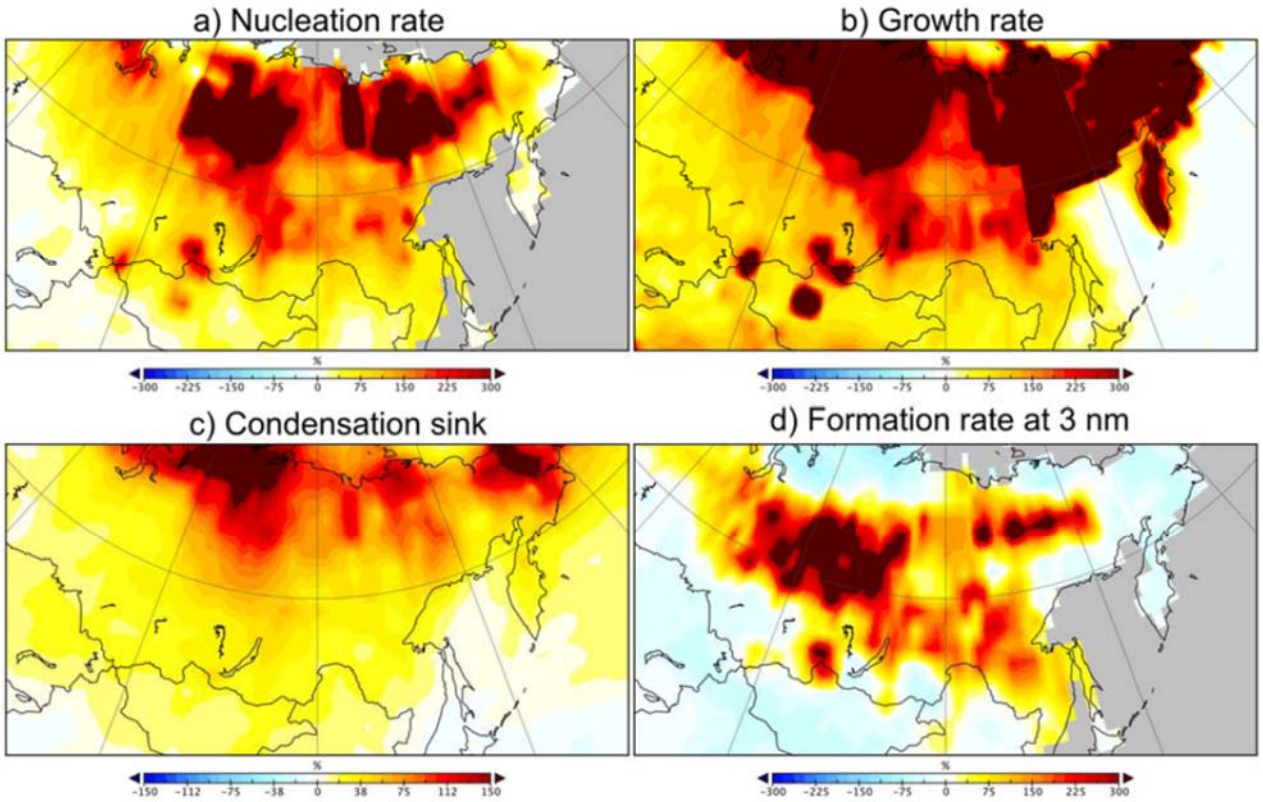

Figure A2: Relative change between years 2000 and 2100 (%) nucleation rate (a), growth rate (b), condensation sink (c) and formation rate of 3 nm particles in response to altered BVOC emissions (see methods).

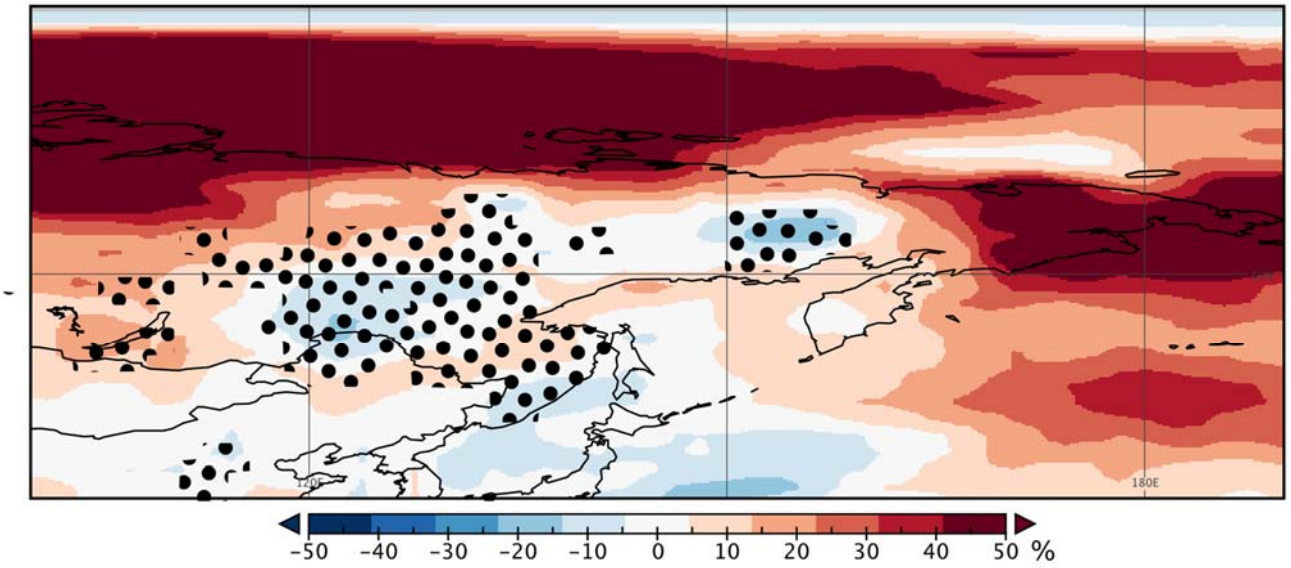

902
903
904

905 **Figure A3**: Relative change in summer average (June-July-August, averaged over five years) CCN(0.2%)
906 concentration in response to altered BVOC emissions (see methods). Dotted areas denote regions where
907 summer wildfire emission exceeds 10^{-11} kg m^{-2} s^{-1} (see Figure 4).
908